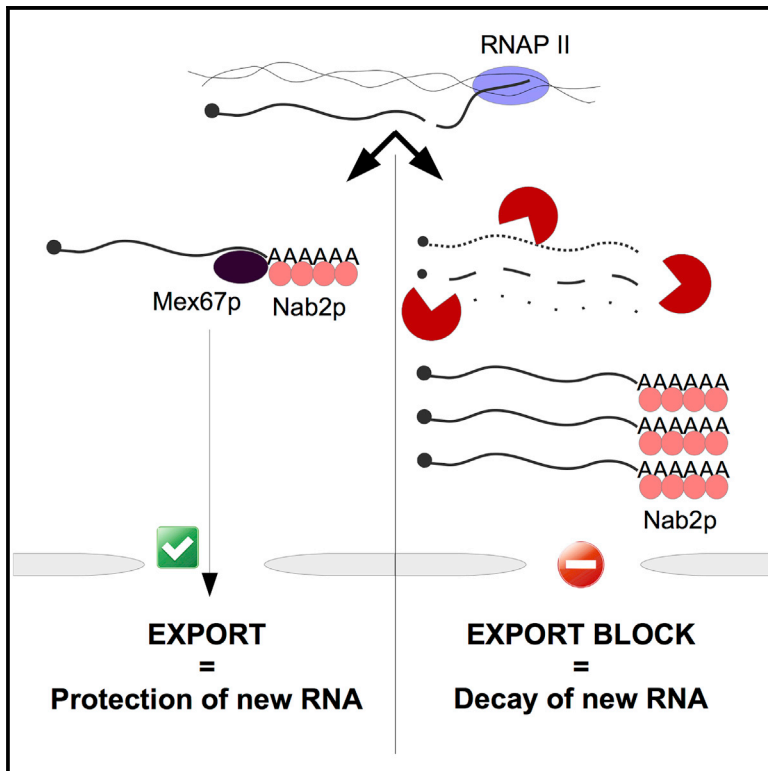


A Nuclear Export Block Triggers the Decay of Newly Synthesized Polyadenylated RNA

Graphical Abstract



Authors

Agnieszka Tudek, Manfred Schmid, Marius Makaras, J. David Barrass, Jean D. Beggs, Torben Heick Jensen

Correspondence

thj@mbg.au.dk

In Brief

Tudek et al. show that nuclear accumulation of existing pA⁺ RNA, due to an export block, results in the out-titration of the pA-binding protein Nab2p away from newly synthesized pA⁺ RNAs. The absence of Nab2p results in transcript decay, which highlights the importance of efficient nuclear export for mRNA stability.

Highlights

- An export block triggers nuclear accumulation of pA⁺ RNA and decay of newly made RNA
- Retained RNA sequesters pA-binding protein Nab2p, preventing protection of new RNA
- Efficient RNA export is essential for cellular mRNA stability



A Nuclear Export Block Triggers the Decay of Newly Synthesized Polyadenylated RNA

Agnieszka Tudek,¹ Manfred Schmid,¹ Marius Makaras,¹ J. David Barrass,² Jean D. Beggs,² and Torben Heick Jensen^{1,3,*}¹Department of Molecular Biology and Genetics, Aarhus University, C. F. Møllers Allé 3, Building 1130, 8000 Aarhus C, Denmark²Wellcome Centre for Cell Biology, University of Edinburgh, Edinburgh EH9 3BF, UK³Lead Contact*Correspondence: thj@mbg.au.dk<https://doi.org/10.1016/j.celrep.2018.07.103>

SUMMARY

Genomes are promiscuously transcribed, necessitating mechanisms that facilitate the sorting of RNA for function or destruction. The polyA (pA) tail is one such distinguishing feature, which in the *Saccharomyces cerevisiae* nucleus is bound by the Nab2p protein, yielding transcript protection. As Nab2p also contacts the main nuclear export factor Mex67p, we asked whether transport kinetics contributes to RNA sorting. Indeed, 3' end sequencing of newly transcribed pA⁺ RNAs demonstrates that nuclear depletion of Mex67p elicits their instant and global decay. A similar phenotype is evident upon inactivation of other export factors and proportional to the amount of nuclear pA⁺ RNA. As RNA expression is partially rescued by Nab2p overexpression, we propose that an export block out-titrates Nab2p onto nuclear-retained pA⁺ RNA, reducing the pool of Nab2p available to protect new transcripts. More generally, we suggest that nuclear RNA decay, negotiated by Nab2p availability, aids in balancing cellular transcript supply with demand.

INTRODUCTION

RNA polymerase II (RNAPII) transcribes a variety of RNAs with different half-lives, reflecting their cellular utilities. In *S. cerevisiae* these include mRNAs as well as several types of non-coding RNAs, such as small nuclear/nucleolar (sn/sno) RNAs, cryptic unstable transcripts (CUTs), stable unannotated transcripts (SUTs), and Xrn1p-sensitive unstable transcripts (XUTs) (Wyers et al., 2005; Xu et al., 2009; van Dijk et al., 2011). Transcription termination at sn/snoRNA and CUT transcription units (TUs) is mediated by the Nrd1p/Nab3p/Sen1p (NNS) complex, which recruits the non-processive Trf4p/Air2p/Mtr4p-polyadenylation (TRAMP) complex to stimulate the 3'-5' exonucleolytic RNA exosome complex for complete decay of CUTs or for the 3' end maturation of sn/snoRNAs (Porrua and Libri, 2015; Vasiljeva and Buratowski, 2006; Wyers et al., 2005). In contrast, transcription termination and 3' end processing of most mRNAs, as well as SUTs and XUTs, depend on the cleavage factor I (CFI)/cleavage and polyadenylation factor

(CPF) complexes that processively add polyA (pA) tails to RNA 3' ends, conferring RNA stability (van Dijk et al., 2011; Porrua and Libri 2015).

In *S. cerevisiae*, pA tail function is mediated by the dedicated pA-binding proteins (PABPs) Nab2p and Pab1p, which at steady state are nuclear and cytoplasmic, respectively. Nab2p binds to the nascent pA tail of newly synthesized RNA (Batisse et al., 2009; Kelly et al., 2007; Kelly and Corbett, 2009; Hector et al., 2002) and remains bound during nuclear export to the cytoplasm, where it is replaced by Pab1p (Green et al., 2002; Aitchison et al., 1996; Tran et al., 2007). Using the anchor-away (AA) technique (Haruki et al., 2008) to rapidly deplete nuclear Nab2p, we recently demonstrated that its binding to nascent pA tails is essential to protect newly made mRNA from decay by the nuclear exosome. *In vitro* Nab2p can physically block exosome access to a polyadenylated substrate (Schmid et al., 2015), but whether this is its main mode of action *in vivo* was not explored. In particular, Nab2p partakes in mRNA nuclear export (Green et al., 2002; Hector et al., 2002; Marfatia et al., 2003; Grant et al., 2008; Iglesias et al., 2010), which might contribute to the timely “escape” of transcripts from the degradative environment of the nucleus.

mRNA nuclear export is mediated by a set of RNA-binding proteins, which converge at the key Mex67p-Mtr2p heterodimer (Segref et al., 1997; Santos-Rosa et al., 1998). Targeting of Mex67p-Mtr2p to transcripts *in vivo* is facilitated by RNA-binding adaptor proteins, such as the SR-like protein Npl3p, the Yra1p subunit of the transcription-export (TREX) complex, and Nab2p. Prior to exit through the nuclear pore complex (NPC), Yra1p dissociates (Gilbert and Guthrie 2004; Iglesias et al., 2010; Hautbergue et al., 2008; Kelly and Corbett, 2009), while the remaining export factors form contacts with nucleoporins (NUPs) of the NPC and stay bound to the mRNA during NPC traversal (Terry and Wente, 2007; Grant et al., 2008). Upon arrival of the messenger ribonucleoprotein (mRNP) at the cytoplasmic side, the Dbp5p helicase is activated by its interaction with the NUP Gle1p (Hodge et al., 1999), which then leads to release of the mRNP into the cytoplasm and relocation of shuttling proteins such as Mex67p-Mtr2p, Npl3p, and Nab2p back into the nucleus (Tran et al., 2007; Lund and Guthrie, 2005).

Interestingly, mutation or depletion of selected mRNA export factors was shown to elicit nuclear exosome-dependent decay of the heat shock (hs)-inducible transcripts *HSP104* and *SSA4* (Rougemaille et al., 2007; Libri et al., 2002; Assenholt et al., 2008; Jimeno et al., 2002). We therefore wondered whether



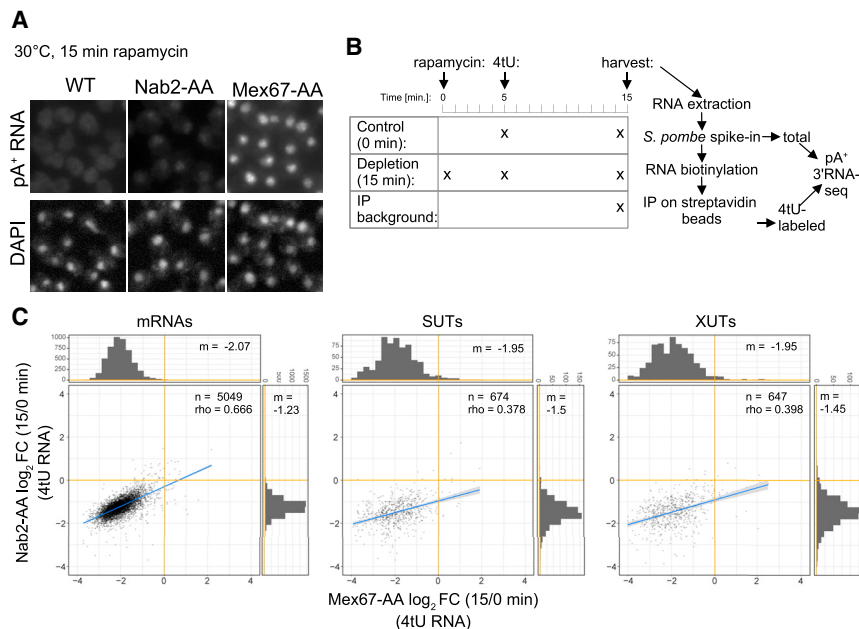


Figure 1. Rapid Nuclear Depletion of Mex67p Results in Global Inhibition of pA⁺ RNA Net Production

(A) Fluorescent *in situ* hybridization (FISH) analysis of pA⁺ RNA using a Cy3-labeled dT18 DNA/LNA probe on fixed WT, Nab2-AA, or Mex67-AA cells subjected to rapamycin treatment for 15 min at 30°C (top). FISH Cy3 images were adjusted to a common display range (defined as the highest and lowest pixel values for the three images) to allow comparison between strain phenotypes. DAPI staining was used to visualize chromatin-rich regions of cell nuclei (bottom).

(B) Schematic workflow of the pA⁺ RNA 3' end sequencing experiment. Mex67-AA and Nab2-AA cultures were treated with 4tU for 10 min (“Control (0min)”) or pre-treated with rapamycin for 5 min before 4tU addition (“Depletion (15 min)”). Cells that were not treated with 4tU or rapamycin were used as reference to estimate the background of the 4tU purification (“IP background”). All obtained RNA samples were supplemented with *S. pombe* spike-in transcripts, biotinylated, and purified on streptavidin beads. Both total and 4tU-purified fractions were subjected to pA⁺ RNA 3' end sequencing.

(C) Log₂ fold changes (FC) of pA⁺ RNA net production in 4tU-labeled Mex67-AA (x axis) and Nab2-AA (y axis) cells treated with rapamycin for 15 min and compared with their respective controls (no rapamycin). Three major pA⁺-containing transcript classes were analyzed: mRNAs, SUTs, and XUTs. Only transcripts purified significantly above background in the control samples are depicted. The number of genes (n), Spearman correlation coefficients (rho), and median (m) values for both datasets are specified on each graph. See also Table S1. See also Figure S1.

this phenotype might reflect a mechanistic aspect of the global mRNA decline observed in Nab2p-depleted cells (Schmid et al., 2015). Here, we show that rapid nuclear depletion of Mex67p compromises production of pA⁺ RNAs by triggering their immediate decay without affecting their transcription. This is a general phenotype triggered by defective nuclear export of pA⁺ RNA, with the degree of transcript decay following the strength of the export block. Finally, we demonstrate increased binding of Nab2p to pA⁺ RNA during an export block and that the associated RNA decay phenotype can be partially rescued by Nab2p overexpression. This suggests that nuclear pA⁺ RNA accumulation depletes the available pool of Nab2p, leaving pA tails of newly produced RNAs unprotected and subject to decay. Our results therefore establish Nab2p as a limiting and essential factor for nuclear mRNA production and highlight the importance of rapid pA⁺ RNA export for gene expression.

RESULTS

Rapid Nuclear Depletion of Mex67p Globally Inhibits the Net Production of New pA⁺ RNA

Because of its tight connection to mRNA export factors, we asked whether the previously demonstrated requirement of Nab2p to protect newly produced mRNA from decay (Schmid et al., 2015) might relate to its role in nuclear export. We therefore compared the phenotypes induced by rapid nuclear depletion of Nab2p and Mex67p by taking advantage of the AA system in which the AA-tagged protein of interest is nuclear depleted following rapamycin addition. As previously described, and

consistent with the essential nature of these proteins, nuclear depletion of Mex67p or Nab2p resulted in cell death (Figure S1A; Haruki et al., 2008; Schmid et al., 2015). Moreover, loss of nuclear Mex67p caused an instant and dramatic nuclear accumulation of pA⁺ RNA (Figure 1A), consistent with the central role of the protein in mRNA export (Santos-Rosa et al., 1998; Haruki et al., 2008). In contrast, nuclear depletion of Nab2p caused only modest pA⁺ RNA accumulation, despite a clear nuclear depletion of the protein (see below), probably because of the presence of other adaptor proteins capable of recruiting Mex67p-Mtr2p. Despite these different pA⁺ RNA localization phenotypes, the abundance of selected mRNAs was significantly decreased in both Mex67- and Nab2-AA, but not wild-type (WT), cells upon rapamycin treatment (Figure S1B). Some transcripts, such as *HHF1*, *HTA2*, *RRP6*, *RPS9A*, and *TLC1*-pA (red-colored series), a precursor of the telomerase component *TLC1*, were decreased as soon as 10 min after rapamycin addition, whereas others, such as *PGK1*, *PMA1*, *TDH3*, *RPL21A*, *RPL36A* (blue-colored series), and *NAB2* (orange color) declined at a slower rate, especially in Mex67-AA cells. In contrast, levels of *SCR1*, a non-adenylated product of RNAPIII, were not down-regulated throughout the course of the experiment. Only very few protein-coding transcripts increased in abundance upon Mex67p depletion. However, this is likely due to special mechanistic circumstances (see below), and the overall initial resemblance of results from Mex67- and Nab2-AA cells encouraged us to compare RNA production in the two strains genome-wide.

Given the specific impact of Mex67p and Nab2p depletion on polyadenylated RNA, we chose to sequence pA⁺ RNA 3' ends

from cells subjected to a brief (15 min) rapamycin exposure, minimizing any secondary effects due to protein inactivation. However, because long-lived transcripts synthesized prior to Mex67p or Nab2p nuclear depletion would mask effects on newly synthesized RNA, we also metabolically labeled cells with 4-thiouracil (4tU) 5 min after rapamycin addition to allow the synthesis of new RNA for 10 min before its specific purification (Figure 1B). We calculated fold changes in mRNAs, SUTs, and XUTs levels between the 15 and 0 min depletion time points for both strains. Two fractions were analyzed, the steady-state transcript levels (Figure S1C, “total RNA”) and RNA “net production” within the 10 min labeling period (Figure 1C, “4tU RNA”), understood as the RNA amount deriving from transcription minus any decay. Mex67-AA and Nab2-AA strains were compared on the x and y axes, respectively. Consistent with previous data (Schmid et al., 2015) and single-transcript analysis (Figure S1B), modest but significant declines in mRNA, SUT, and XUT levels were observed in the total RNA fraction upon nuclear depletion of Mex67p or Nab2p (Figure S1C). Importantly, this drop in expression was greatly exacerbated in the 4tU-labeled fractions (Figure 1C).

Although the effects of Nab2p nuclear depletion on mRNA levels and net production were quantitatively weaker than those of the Mex67p depletion, the response triggered was qualitatively similar, with Spearman correlation coefficients of 0.588 between the two total fractions (Figure S1C) and 0.666 between the 4tU-labeled samples (Figure 1C). Changes in SUT and XUT expression correlated less strongly between samples but showed globally similar downregulation. The more robust depletion effect seen for the 4tU-labeled samples validated the quality of the 4tU RNA purification and indicated that the observed phenotypes were caused by an impairment of *de novo* pA⁺ RNA net production rather than accelerated decay of pre-existing cytoplasmic transcripts. These conclusions were reinforced by the observation that downregulation of mRNA levels were in agreement with cytoplasmic decay rates considering the total, but not the 4tU-labeled, fractions (Figure S1D). This was the case for both published data (Sun et al., 2012; Presnyak et al., 2015; Miller et al., 2011) and estimates derived from our own data. In other words, a decline in levels of short-lived transcripts could readily be observed in the total fraction, whereas individual transcript half-lives had no relation to the strength of new pA⁺ RNA net production inhibition. We conclude that nuclear depletion of Mex67p and Nab2p results in a rapid and strong genome-wide inhibition of the net production of transcripts from CFI/CPF-dependent TUs.

Decreased pA⁺ RNA Net Production in Mex67p- and Nab2p-Depleted Cells Is Due to Increased Transcript Decay

The massive downregulation of pA⁺ RNA net production in Nab2p and Mex67p nuclear-depleted cells could be due to either a global transcriptional shutdown or rapid decay of newly made RNA. We did not observe any substantial correlation between the degree of 4tU RNA downregulation in Nab2p or Mex67p nuclear-depleted cells and various published transcription estimates (Figure 2A; Mayer et al., 2010; Warfield et al., 2017; Churchman and Weissman 2011; Milligan et al., 2016), suggesting that the decrease in pA⁺ RNA net production occurs

post-transcriptionally. Nevertheless, to irrevocably address this critical question, we evaluated transcription levels of the affected strains, using a 2 min pulse of 4tU labeling followed by the simultaneous detection of mature pA⁺ RNA and nascent pA⁻ 3' ends (Figure 2B), the latter constituting a reliable transcription measure (Schmid et al. 2018 [this issue of *Cell Reports*]).

Sequence reads mapped across five regions of chromosomes I, III, VI, and VII (Figures 2C and S2A) demonstrated that pA⁺ 3' ends from 4tU-labeled samples mainly detected the annotated 3' ends of the relevant mRNAs, whereas pA⁻ 3' ends were scattered along the analyzed TUs. Summing pA⁻ reads mapping to protein-coding gene bodies (from transcription start sites [TSSs] to 200 bp upstream of transcript end sites [TESs]) thus yielded a transcription estimate, whereas pA⁺ reads mapping to gene ends (TES \pm 200 bp) yielded an estimate of mature pA⁺ RNA net production. A subsequent comparison of mRNA gene body pA⁻ 3' end read densities between rapamycin-treated and untreated Mex67-AA and Nab2-AA cells showed only modest differences (Figures 2C, 2D, and S2A). Consistently, chromatin immunoprecipitation (ChIP) of the RNAPII subunit Rbp3p on selected downregulated genes did not reveal any major changes between control and Mex67p nuclear-depleted cells (Figure S2B, gray series). In contrast, pA⁺ 3' ends were robustly downregulated in the 4tU-labeled fractions as a consequence of nuclear depletion of either Mex67p or Nab2p (Figures 2C, 2D, and S2A), demonstrating that mRNA net production was diminished despite virtually unaltered transcription. We therefore conclude that nuclear depletion of Mex67p or Nab2p triggers the rapid decay of newly produced pA⁺ RNA.

We then asked which nuclease might be responsible. Examination of new RNA production in a Mex67-AA/*rrp6* Δ background did not reveal any substantial rescue (Figure S2C). Simultaneous depletion of both exosome nucleases, Rrp6p and Dis3p, resulted in the predicted stabilization of its *NEL025c* target (Figure S2D) but did not rescue the decay of new hs RNAs under export block conditions (Figure S2E). We then turned to depletion, via the auxin-inducible degron (AID; Morawska and Ulrich, 2013), of one or both of the major yeast 5'-3' nucleases, the predominantly cytoplasmic Xrn1p and the nuclear Rat1p enzymes. This yielded strains with the predicted stabilization of 3' extended read-through fragments of two selected mRNAs (Figure S2F). However, when examining total RNA levels from Rat1-AID/Mex67-AA or Rat1-AID/Xrn1-AID/Mex67-AA cells (Figure S2G), only mild rescue of some RNA levels could be detected. We conclude that neither of the tested nucleases is solely responsible for the decay of new RNA. Yet another enzyme might partake in the decay or, perhaps more likely, degradation is performed redundantly by several nuclear decay factors.

Inspection of our data also revealed increased levels of pA⁻ 3' end signals downstream the TESs of many protein-coding genes in Mex67p nuclear-depleted cells, which was less visible in Nab2p-depleted cells (Figure S2H). This implied the rapid induction of a transcription termination defect upon Mex67p inactivation, which was previously observed on reporter genes (Hammell et al., 2002) and verified by RT-qPCR analysis of 3' extended RNAs derived from the *HHF1*, *RPL36A*, and *TDH3* genes (Figure S2I, green series). As 3' extended transcripts are usually labile (Minvielle-Sebastia et al., 1991; Libri et al., 2002), we

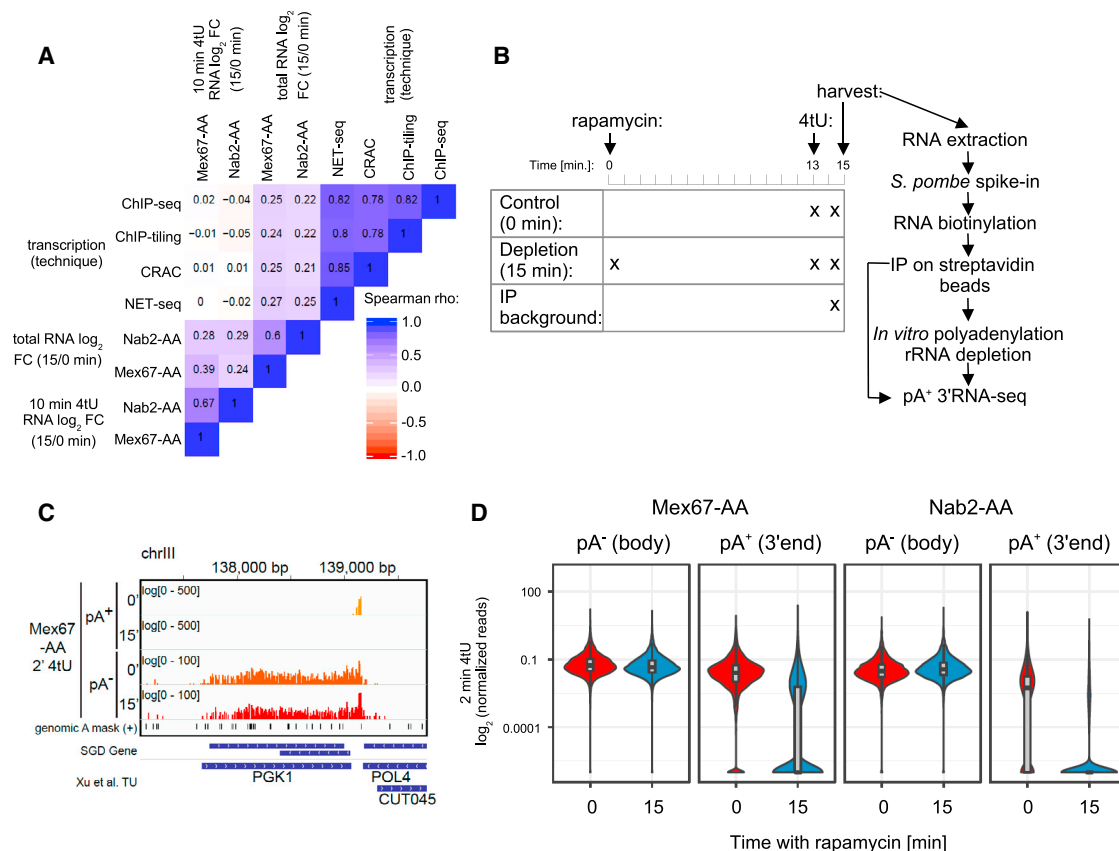


Figure 2. Decreased pA⁺ RNA Net Production in Mex67p- and Nab2p-Depleted Cells Is Due to Increased Transcript Decay

(A) Spearman correlation coefficient matrix comparing mRNA log₂ FC of 15/0 min rapamycin ratios in Mex67- and Nab2-AA cells as in Figures 1C and S1C against various estimates of transcription rates. Transcription estimates were derived from RNAPII NET-seq (Churchman and Weissman 2011), RNAPII-CRAC (Milligan et al., 2016), RNAPII-ChIP-seq (Warfield et al., 2017), and RNAPII-ChIP-tiling (Mayer et al., 2010) data.

(B) Schematic workflow of the pA⁺/pA⁻ RNA 3' end sequencing experiment. Cells were treated with 4tU for 2 min. In case of the Mex67-AA- and Nab2-AA-depleted cells, cultures were pre-treated with rapamycin for 13 min before 4tU labeling. Addition of *S. pombe* spike-in RNAs, biotinylation, and purification of 4tU-labeled RNA were done as described in Figure 1B. Samples were then split in two aliquots, in which one was subjected to pA⁺ RNA 3' end sequencing as in Figure 1B, and the other was *in vitro* polyadenylated and rRNA-depleted prior to pA⁺ RNA 3' end sequencing.

(C) Genome Browser view of spike-in normalized pA⁻ and pA⁺ RNA 3' end reads derived from 2 min 4tU-labeling experiments of untreated (0') and 15 min nuclear-depleted (15') Mex67-AA cells, spanning across the gene-coding strand of *PGK1* on chromosome III. Annotations below the tracks show genomic A-rich sites masked in the analysis and boundaries of translated and transcribed regions as previously defined in www.yeastgenome.org and Xu et al. (2009), respectively.

(D) Levels of nascent ("pA⁻ (body)") and mature ("pA⁺ (3' end)") mRNAs in 2 min 4tU-labeled samples in Mex67-AA (left) and Nab2-AA (right) cells after 0 (red violins) or 15 (blue violins) min of rapamycin treatment. All signals are shown relative to *S. pombe* spike-ins, with background subtracted, log₂ and length scaled. Levels of transcripts that were not purified above background were set to a pseudocount of 10⁻⁶. Violin plots shown are overlaid with box plots depicting the median values with boxes demarcating first and third quartiles of the data. See also Table S2.

See also Figure S2.

considered the possibility that newly made pA⁺ RNAs in Mex67p-depleted cells were unstable because of this transcription termination defect. However, not all loci showed an increased signal downstream of their TESSs, and there was only a marginal negative correlation between the severity of the defect and the extent to which the same mRNA was downregulated (Figures S2H and S2J). This argued against a general causative link between the phenotypes and suggested that transcription termination defects only contribute to RNA decline in selected cases. Still, a termination defect, though of a different type, may explain the aforementioned stabilization of a small set of RNAs. The upregulation of one such target in Mex67p-

depleted cells, the *NRD1* mRNA (Figure S2I, red bar), was for example likely due to a transcription termination defect at the NNS-responsive region positioned in the 5' end of the *NRD1* gene (Porrua and Libri, 2015). Consistent with this notion, RNAPII ChIP levels increased specifically downstream of the *NRD1* gene NNS site upon Mex67p nuclear depletion (Figure S2B, compare *NRD1* 5' end with 3' end). We also observed stabilization of several CUTs (Figure S2I, orange series). This was seemingly not caused by decreased Rrp6p levels, which remained unaffected up to 60 min of Mex67p or Nab2p nuclear depletion (Figure S2K). Instead, analysis of pA⁻ reads revealed increased density downstream of many CUT loci (Figure S2L),

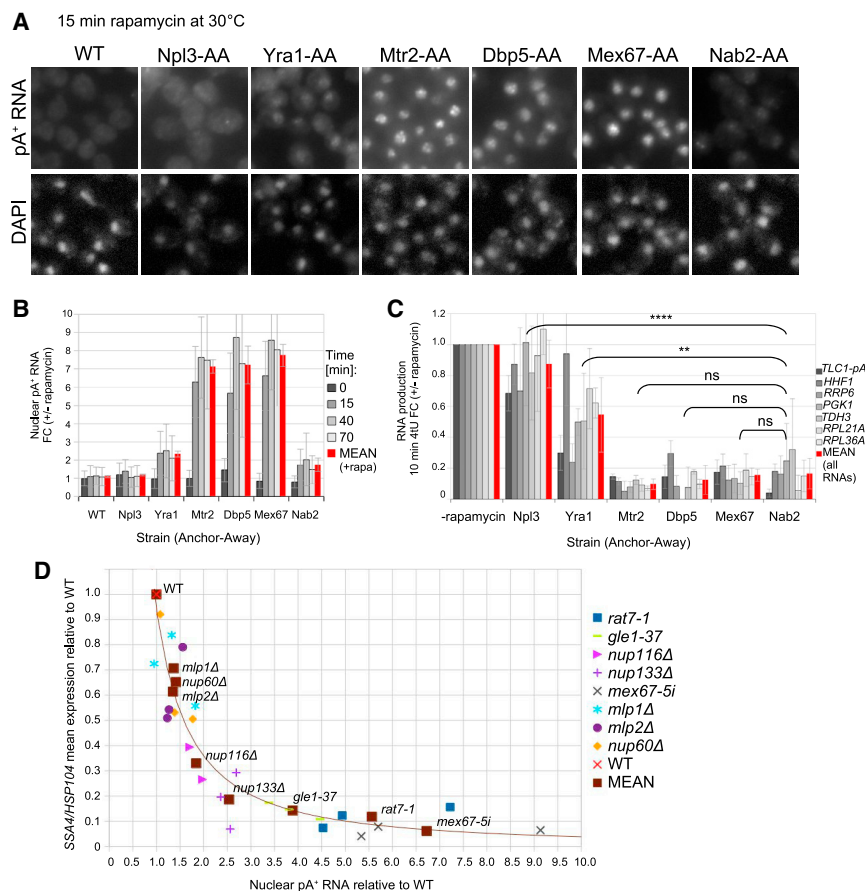


Figure 3. Decreased mRNA Net Production Correlates with the Severity of the Nuclear Export Block

(A) FISH analysis of pA⁺ RNA as in Figure 1A on fixed WT, Npl3-, Yra1-, Mtr2-, Dbp5-, Mex67-, and Nab2-AA cells subjected to rapamycin for 15 min at 30°C. Images were adjusted and stained with DAPI as in Figure 1A. WT, Mex67-AA, and Nab2-AA cells were from the same experiment shown in Figure 1A.

(B) Quantification of nuclear pA⁺ RNA signals of AA cells from (A) incubated for 0, 15, 40, or 70 min with rapamycin. Values are shown relative to mean values of non-rapamycin-treated cells and corrected for background. Error bars at individual time points indicate SDs calculated from nuclear pA⁺ RNA levels of a minimum of 800 cells counted for each strain. Error bars of mean values indicate SDs on the mean accumulation of pA⁺ RNA over the time course of each protein depletion.

(C) RT-qPCR analysis of selected 4tU RNAs of cells from (A). RNA was harvested after 10 min of 4tU labeling. All values were normalized to *S. pombe* spike-in, background-subtracted, and displayed relative to respective non-rapamycin-treated samples. Nab2-, Mex67-, Mtr2-, and Dbp5-AA cells were treated with rapamycin for 15 min, whereas Yra1- and Npl3-AA cells were subjected to rapamycin for 30 min to ensure complete nuclear depletion of these proteins. The mean value of all tested RNAs is indicated in red. Error bars indicate SDs from three to nine biological replicates. Error bars on mean values indicate SD from means of all tested transcripts. qPCR results were analyzed using a two-tailed paired t test for the comparisons indicated in the figure (see STAR Methods details for p value

thresholds). Mean RNA production rate for Mex67-AA was calculated from nine replicate samples, six of which are depicted in Figure 4D. (D) Relationship between levels of nuclear accumulation of pA⁺ RNA (x axis) and the mean of *HSP104* and *SSA4* RNA expression (y axis) in the indicated mutants strains relative to the WT control. Single repeats for each strain are shown separately. The mean of replicates from the individual strains is indicated and labeled and a power function has been fitted to the dataset. See also Figure S3.

consistent with read-through transcription as observed at the *NRD1* locus. This suggests that NNS-mediated transcription termination is, to some extent, also perturbed upon Mex67p nuclear depletion (see Discussion).

Decreased mRNA Net Production Correlates with the Severity of the Nuclear Export Block

Previous studies using mutated variants of diverse mRNA export factors found hs RNA expression to be impaired during an export block (Rougemaille et al., 2007; Libri et al., 2002; Assenbolt et al., 2008; Jimeno et al., 2002). As this phenotype is reminiscent of what we observed upon Nab2p and Mex67p nuclear depletion, decay of newly made pA⁺ RNA might be a general phenotype linked to export factor inactivation. To test this prediction, we tagged the Mex67p cofactor Mtr2p, the export adaptors Yra1p and Npl3p, and the NPC-associated RNA helicase Dbp5p with the AA epitope and analyzed the phenotypic consequences of nuclear depletion of these proteins.

Rapamycin addition to Mtr2-AA, Yra1-AA, and Dbp5-AA cells resulted in their lethality, whereas Npl3-AA cells were severely

growth impaired (Figure S3A), as expected (Bossie et al., 1992; Portman et al., 1997; Hodge et al., 1999; Santos-Rosa et al., 1998). We next compared the pA⁺ RNA localization profiles of the AA strains after 15, 40, and 70 min of rapamycin treatment (Figures 3A and 3B). Depletion of Mtr2p and Dbp5p yielded a “Mex67-AA-like” effect with severe nuclear pA⁺ RNA accumulation (6- to 9-fold) 15 min post-rapamycin addition. In contrast, loss of nuclear Yra1p resulted in more modest pA⁺ RNA accumulation and depletion of Npl3p did not yield a detectable phenotype, despite severely diminished nuclear Npl3p levels (Figure S3B). Interestingly, all mutant-specific pA⁺ RNA localization profiles were essentially established already after 15 min of rapamycin treatment, reaching a plateau thereafter (Figure 3B). Thus, a mutant-specific steady-state concentration of nuclear pA⁺ RNAs is established rapidly, likely reflecting the extent of the export defect. In order to evaluate a possible connection to mRNA synthesis, we employed 4tU labeling to measure the net production of selected mRNAs and found it to be decreased to largely equal extents in Nab2-, Mex67-, Mtr2-, and Dbp5-AA cells after 15 min depletion (Figure 3C). Despite a longer

(30 min) nuclear depletion, loss of Yra1p yielded a more modest phenotype, whereas Npl3p depletion only very mildly impaired mRNA net production. We conclude that depletion of all tested export factors resulted in decreased mRNA net production, which, with an apparent exception of Nab2p-depleted cells, appeared related to the degree of the nuclear pA⁺ RNA export phenotype.

In an attempt to strengthen this relationship, we compared the nuclear pA⁺ RNA accumulation and new mRNA net production profiles in a panel of mutants affecting NPC function. A WT strain and the *mex67-5i* mutant (Jimeno et al., 2002) were taken as reference points and compared with NPC mutants *nup116Δ*, *nup133Δ*, *nup60Δ*, *rat7-1*, and *gle1-37* (Strahm et al., 1999; Jimeno et al., 2002; Lund and Guthrie, 2005; Terry and Wente, 2007; Doye et al., 1994; Gorsch et al., 1995), of which the latter two are directly implicated in Dbp5p function (Hodge et al., 1999). Moreover, we included the nuclear basket deletion mutants *mlp1Δ* and *mlp2Δ* (Strambio-de-Castillia et al., 1999) in the analysis. Because most of these aberrations are permissive at normal growth temperature (25°C–30°C), we assayed nuclear pA⁺ RNA accumulation after incubation at 38°C for 12 min and compared this with the expression of the *HSP104* and *SSA4* hs-inducible RNAs. This revealed a tight correlation between the analyzed nuclear RNA accumulation and mRNA net production phenotypes (Figures 3D and S3C). Strains with modest 1.2- to 1.4-fold increases of nuclear pA⁺ RNA (*mlp1Δ*, *mlp2Δ*, and *nup60Δ*), compared with WT, showed only a mild (~30%) drop in hs RNA expression, whereas cells showing more than 2-fold increases in nuclear pA⁺ RNA (*nup116Δ*, *nup133Δ*, *rat7-1*, and *gle1-37*) exhibited RNA expression decreases of ~80%, similar to *mex67-5* cells (Figure 3D). We conclude that the severe downregulation of new RNA net production correlates well, albeit in a non-linear manner, with the degree of nuclear pA⁺ RNA accumulation.

Nab2p Is Sequestered on Nuclear-Retained RNA in Export-Deficient Cells, and Excess Nab2p Can Alleviate mRNA Downregulation

Given the strikingly similar mRNA net production phenotypes of cells debilitated in nuclear export and depleted of nuclear Nab2p, which causes only a mild export defect, we wondered whether Nab2p activity might be compromised in export-deficient conditions. Immunofluorescence (IF) and ChIP analysis of Nab2p demonstrated that its predominantly nuclear localization was not altered, and the amount of chromatin-bound Nab2p was not decreased upon Mex67p nuclear depletion (Figures S4A and S4B). Nevertheless, we wondered whether Nab2p might be sequestered on pA⁺ RNAs accumulating in the nucleus during an export block and hence be unavailable to yield protection to newly made transcripts. To test this idea, we purified RNAs associated with Nab2p from ± rapamycin-treated Mex67-AA cells, which had been UV cross-linked with 0, 300, or 700 J/cm². Purified Nab2p and its associated P³²-labeled RNA were then resolved by SDS-PAGE (Figure 4A) and both total co-purified RNA (Figure 4A, lanes 1–7) and the RNaseA/T1-resistant pool directly linked to Nab2p (Figure 4A, lanes 8–14) were quantified (Figures 4B and 4C, respectively). Nab2p purified from rapamycin-treated and export-blocked

cells associated with significantly more RNA than the Nab2p isolated from the control condition. Moreover, Nab2p cross-linking attained the maximum efficiency at lower energies during the export block, reflecting the increased amount of binding sites due to nuclear pA⁺ RNA accumulation. These results therefore suggest that Nab2p is indeed sequestered by RNAs accumulating in nuclei. Following this conclusion, it is likely that Mex67p and Nab2p act cooperatively to prevent nuclear decay of pA⁺ RNA. To test this assumption further, we attempted to co-deplete Mex67p and Nab2p from the nucleus by simultaneously AA-tagging these factors. This resulted in some redistribution of Nab2p from the nucleus (Figure S4C), which was incomplete, presumably because both regular Nab2p export and ribosome export, required for the AA system, depend on nuclear Mex67p (Iglesias et al., 2010; Yao et al., 2007). The pA⁺ RNA accumulation phenotype upon Mex67p/Nab2p double depletion was comparable with that of Mex67p-depleted cells (Figure S4D), and a parallel 4tU-labeling experiment demonstrated that the double depletion did not impair mRNA net production more than nuclear depletion of Mex67p alone (Figure 4D, compare RNA series 2 and 3). Together this indicates that Mex67p and Nab2p act in the same pathway.

Previous *in vitro* experiments demonstrated that Nab2p can protect pA⁺ RNA from decay independent of cofactors (Schmid et al., 2015). Hence, lack of Mex67p, or other ways of compromising pA⁺ RNA nuclear export, likely impairs the function of endogenous Nab2p indirectly, in line with the idea that Nab2p is sequestered on accumulating pA⁺ RNA. If this is the case, providing excess Nab2p should alleviate mRNA decay in Mex67-AA cells, and we therefore examined the effect of Nab2p overexpression *in vivo*. Introducing the entire *NAB2* locus on a high-copy 2μ plasmid translated only into a roughly 2- to 3-fold increase of Nab2p levels (Figure 4E), probably reflecting auto-regulatory mechanisms counteracting its overexpression (Roth et al., 2009). Even so, 4tU-labeling analysis demonstrated that net production of selected mRNAs was on average 2-fold more efficient upon such Nab2p overexpression (Figure 4D, compare RNA series 3 and 4). To increase Nab2p overexpression even further, we placed the *NAB2* ORF behind a galactose-inducible promoter, which attained its full capacity within 6 hr of galactose induction (Figure 4F). Prolonged Nab2p overexpression revealed to be toxic to cell growth (Figure S4E), and we therefore induced Nab2p expression for 2.5, 5, 6, and 8 hr before monitoring its effect on new RNA production, which again revealed a partial rescue (Figure 4D, compare series 5 with 6, 7, 8, and 9). Even though the rescue was still not complete, we note that it was on average more robust than when expressing Nab2p from the 2μ plasmid (Figure S4F). These results collectively support the notion that nuclear Nab2p levels are limiting in Mex67p-depleted cells and thus insufficient to support normal mRNA net production.

DISCUSSION

The compromised net production of new pA⁺ RNA, resulting from export inhibition, occurs without a significant decrease in cellular transcription levels, demonstrating an extensive decay

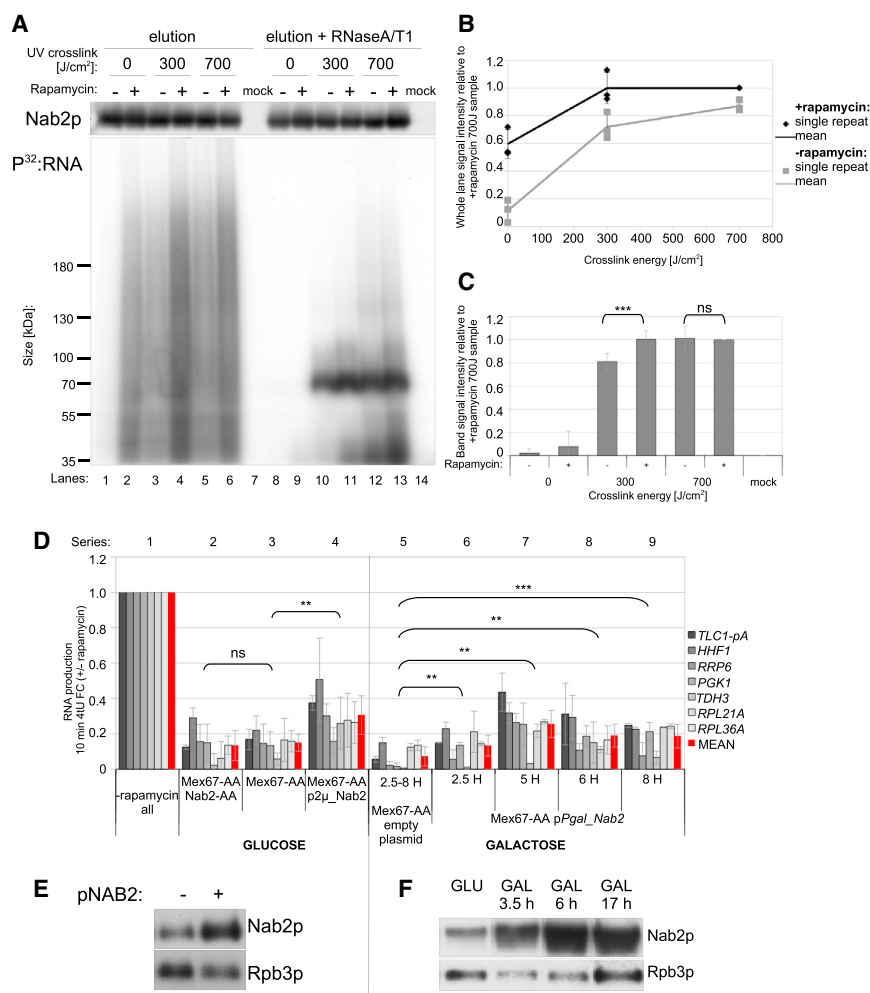


Figure 4. Nab2p Is Sequestered on Nuclear-Retained RNA in Export-Deficient Cells and Excess Nab2p Can Alleviate mRNA Downregulation

(A) SDS-PAGE of eluted samples from an RNA immunoprecipitation (IP) experiment in which endogenous Nab2p was immunoprecipitated from Mex67-AA cells without (“rapamycin -”) or treated with rapamycin for 30 min (“rapamycin +”). Before RNA IP, cells were not subjected to crosslinking (“0 J/cm²”), moderately cross-linked (“300 J/cm²,” ~2 min cross-linking time), or strongly cross-linked (“700 J/cm²,” ~5 min cross-linking time). Mock samples were negative control IPs using beads without anti-Nab2p antibody. Shown are IP eluates without (lanes 1–7) or with (lanes 8–14) prior RNaseA/T1 treatment. Top: western blotting analysis of Nab2p levels; bottom: autoradiogram of P^{32} -labeled SDS-PAGE gel (representative example of three independent repeats).

(B) Quantification of the P^{32} -labeled RNA signal from lanes 1–7 in (A). Background was estimated and subtracted on the basis of the mock sample. Single points represent values obtained from three individual repeats. Error bars represent SDs.

(C) Quantification of P^{32} -labeled RNA signal within the Nab2p contained band of lanes 8–14 from (A). Values were normalized as in Figure 4B. Error bars represent SDs from three independent repeats, and statistical significance was tested using a two-tailed paired t test.

(D) RT-qPCR analysis of selected 10 min 4tU-labeled RNAs purified from cells treated for 15 min with rapamycin as in Figure 3C. RNA series 2–4 show new RNA production from control Mex67-AA cells grown in glucose (series 3), which have been simultaneously depleted for Nab2p (Mex67-AA/Nab2-AA) (series 2) or containing a Nab2p expressing plasmid (Mex67-AA p2 μ _NAB2) (series 4). Values derive from a minimum of four biological replicates, and error bars indicate SDs. Values for

RNA series 3 were also included in the mean shown in Figure 3C. RNA series 5–9 show new RNAs from Mex67-AA cells containing an empty (series 5) or a pPgal_Nab2 (series 6–9) plasmid and incubated for 2.5, 5, 6, or 8 hr in galactose. Values are a mean of two biological replicates for the pPgal_Nab2 containing samples and an average of single replicates for the empty plasmid sample. Error bars indicate median absolute deviation.

(E) Western blotting analysis of Nab2p levels in non-rapamycin-treated Mex67-AA cells transformed with either an empty 2 μ pRS426 plasmid (-) or its counterpart (pNAB2) expressing wild-type Nab2p (+). Rpb3p served as a loading control.

(F) Western blotting analysis showing Nab2p and Rpb3p levels in cells containing a NAB2 gene under control of a galactose-inducible promoter (pPgal_Nab2) in glucose (GLU) condition and at the indicated times after galactose (GAL) addition. The image was edited to show only one of the repeats performed in parallel. See also Figure S4.

of new RNAs in these conditions. The phenotype is robust regardless of the cause of the imposed nuclear export block and does not depend on initial transcription levels of the affected loci. Together, this suggests a post-transcriptional mechanism preventing excessive accumulation of nuclear pA⁺ RNA and that timely mRNA export is important, not only for protein production but also to prevent nuclear decay.

The decline in new pA⁺ RNA net production is tightly related to the amount of nuclear-retained pA⁺ RNA. Hence, even slight increases in nuclear pA⁺ RNA lead to significantly decreased new RNA production. This implies a critical need for cells to keep their nuclear pA⁺ RNA concentrations low, which is perhaps instigated because Nab2p levels are limiting and constantly must be recycled from the cytoplasm. Our data

support this possibility, as they show a strong correlation between the decay phenotypes elicited by nuclear depletion of Mex67p and Nab2p, despite the weak contribution of Nab2p to pA⁺ RNA export. Considering that Nab2p binding to nascent pA tails protects the transcripts from degradation (Schmid et al., 2015), we propose that nuclear accumulation of pA⁺ RNP leads to the out-titration of Nab2p, preventing the protein from protecting newly made RNA and thus eliciting their degradation similarly to conditions of Nab2p nuclear depletion (Figure 5, bottom left). This model is strongly supported by the fact that Nab2p isolated from export-blocked cells binds more RNA than in the WT situation and that effects of depletion of both Mex67p and Nab2p are not additive. Nab2p overexpression can rescue the RNA decay phenotype, indicating

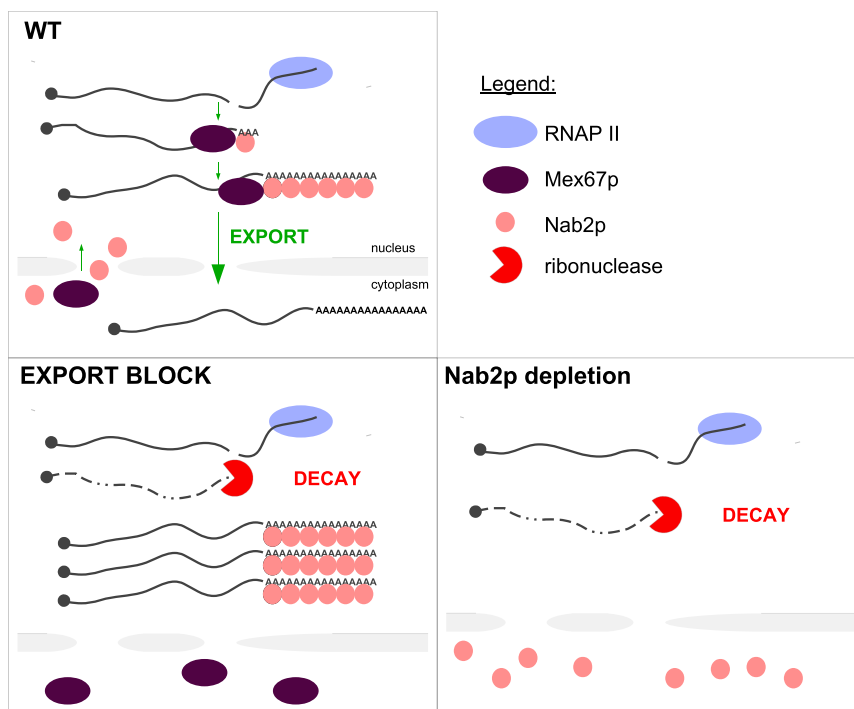


Figure 5. Nuclear RNA Export Block Sequesters Nab2p on Retained RNAs and Elicits the Decay of Newly Made Transcripts

Model for the decay of newly synthesized pA⁺ RNA in export compromised cells. In normal conditions (“WT”), Nab2p protects newly made transcripts and stimulates Mex67p-mediated nuclear export (top). When pA⁺ RNA export is compromised (“EXPORT BLOCK”), Nab2p is inactivated, likely by getting sequestered on retained pA⁺ RNA (bottom left). Hence, Nab2p is unavailable to protect newly made transcripts, leading to their decay, similarly to conditions of Nab2p nuclear depletion (bottom right).

also explain why nuclear depletion of Mex67p leads to a stronger phenotype than nuclear loss of Nab2p. In Nab2p-depleted cells, where pA⁺ RNA export is only mildly affected, newly made transcripts are only exposed to the nuclear degradative environment for a brief time period. In Mex67p-depleted conditions, however, new pA⁺ RNAs are not only labile, because of the limiting supply of Nab2p, but also trapped in the nucleus.

Together with the pronounced nuclear pA⁺ RNA accumulation in Mex67p-depleted cells, which might also cause shortage of other protective factors, this would create additional decay opportunities, not relevant in the Nab2p-depleted nuclei. Regardless of the exact mechanism of decay, our results demonstrate that maintenance of a low nuclear pA⁺ RNA concentration is key to proper pA⁺ RNA production. Under normal conditions, cells prevent nuclear pA⁺ accumulation by rapid export, whereas RNA decay provides a fail-safe mechanism when export is weakened. Mechanistically, these functions are tightly connected as Nab2p facilitates both the loading of Mex67p on nascent RNA while simultaneously yielding physical protection from decay.

Regulation of cellular mRNA levels by transcription and cytoplasmic decay has been extensively studied (Castells-Roca et al., 2011; Parker, 2012), whereas contributions from nuclear decay have been reported only recently (Roy and Chanfreau, 2014; Bresson et al., 2017). The strict requirement for Nab2p to confer stability to newly made pA⁺ RNA raises the possibility of a broader function of this protein in “monitoring” cellular mRNA levels. Nab2p participates in the regulation of its own mRNA (Roth et al., 2009), suggesting that controlling the concentration of this protein is critical. Future efforts will focus on possible roles of Nab2p in affecting cellular pA⁺ RNA homeostasis, which could be especially important during switches in growth programs, such as during starvation or stress, which require global changes of transcription rates (Castells-Roca et al., 2011; Bresson et al., 2017). Our results positioning Nab2p and nuclear export as a limiting factor for mRNA production therefore invite speculation as to whether changes in the abundance or sub-cellular localization of Nab2p might partake in such responses.

that, in accordance with previous *in vitro* results (Schmid et al., 2015), the protein performs an RNA protective function. This rescue is not strictly proportional to Nab2p levels, perhaps because of detrimental effects of its overexpression or due to an impact of other mRNP protective proteins, which might also become limiting during an export block.

Some CUTs, the *NRD1* mRNA and numerous 3' extended mRNAs, are upregulated in Mex67p but less strongly in Nab2p nuclear-depleted cells, which indicates impaired NNS and CFI/CPF functions in the absence of Mex67p. Because levels of 3' extended mRNAs do not correlate with the extent of the decline of their corresponding mRNAs, they cannot be causative for the phenotype. Rather, we suggest that CFI/CPF and NNS complexes are also, at least partially, sequestered on nuclear-retained pA⁺ RNA and therefore cannot efficiently perform their co-transcriptional functions. More generally, such sequestration of nuclear RNP proteins may be widespread during a nuclear export block, further highlighting the necessity of rapid nuclear RNA clearance, either by export of functional molecules or by decay.

What then is the mechanism of removal of newly produced pA⁺ RNA in export-deficient cells? It was previously shown that deletion of the nuclear exosome component *RRP6* partially restores mRNA levels and rescues the lethality of Nab2p-deficient cells (Schmid et al., 2015). However, we were unable to rescue new mRNA production in Mex67p nuclear-depleted cells by impairing nuclear exosome function or depleting the 5'-3' exonucleases Rat1p or Xrn1p. Even though it is possible that another undisclosed nuclear nuclease is solely responsible, we find it more likely that nuclear decay systems act redundantly to remove these transcripts. This would

STAR★METHODS

Detailed methods are provided in the online version of this paper and include the following:

- **KEY RESOURCES TABLE**
- **CONTACT FOR REAGENT AND RESOURCE SHARING**
- **EXPERIMENTAL MODEL AND SUBJECT DETAILS**
 - Yeast strains, growth conditions and plasmids
- **METHOD DETAILS**
 - RNA extraction, reverse-transcription and qPCR
 - ChIP of Nab2p and Rpb3p
 - Nab2p RNA immunoprecipitation (RIP)
 - Isolation of newly synthesized RNAs using 4tU labeling
 - Western blotting analysis
 - pA⁺ RNA FISH analysis and protein localization
 - pA⁺ RNA 3' end sequencing and bioinformatics analysis
 - Bioinformatics
 - RNA 3' end sequencing quality control, filtering, mapping and normalization
 - Annotations
 - Counting gene body and end signal
 - Differential expression analysis
 - Metagene heatmaps
 - Correlation between RNA net production and published transcription and decay-rate data
- **QUANTIFICATION AND STATISTICAL ANALYSIS**
- **DATA AND SOFTWARE AVAILABILITY**

SUPPLEMENTAL INFORMATION

Supplemental Information includes four figures and three tables and can be found with this article online at <https://doi.org/10.1016/j.celrep.2018.07.103>.

ACKNOWLEDGMENTS

We thank Marta Lloret Llinares, Toomas Silla, Tommaso Villa, and Domenico Libri for critical comments on the manuscript. Work in the Jensen laboratory was supported by the Danish National Research Council, the Lundbeck Foundation, and the European Research Council (ERC) (grant 339953). J.D. Beggs was supported by a Wellcome Investigator Award (104648) and a Wellcome Centre for Cell Biology core grant (092076). We thank Logan Decker, Rikke Jespersen, Dorthe Caroline Riisshøj, Aleksandra Biliska, and Ruta Bernotaite for technical support.

AUTHOR CONTRIBUTIONS

A.T., M.S., and T.H.J. conceived the project. A.T. designed, conducted, and analyzed the experiments. M.S. contributed to the 4tU-labeling experiments and performed the bioinformatics analysis. M.M. contributed to RNA fluorescence *in situ* hybridization (FISH) analysis. J.D. Barrass and J.D. Beggs provided advice with 4tU labeling and manuscript corrections. T.H.J. supervised the project. A.T., M.S., and T.H.J. wrote the manuscript.

DECLARATION OF INTERESTS

The authors declare no competing interests.

Received: December 27, 2017

Revised: May 31, 2018

Accepted: July 30, 2018

Published: August 28, 2018

REFERENCES

- Aitchison, J.D., Blobel, G., and Rout, M.P. (1996). Kap104p: a karyopherin involved in the nuclear transport of messenger RNA binding proteins. *Science* *274*, 624–627.
- Anders, S., Pyl, P.T., and Huber, W. (2015). HTSeq—a Python framework to work with high-throughput sequencing data. *Bioinformatics* *31*, 166–169.
- Assenholt, J., Mouaikel, J., Andersen, K.R., Brodersen, D.E., Libri, D., and Jensen, T.H. (2008). Exonucleolysis is required for nuclear mRNA quality control in yeast THO mutants. *RNA* *14*, 2305–2313.
- Barrass, J.D., Reid, J.E., Huang, Y., Hector, R.D., Sanguinetti, G., Beggs, J.D., and Granneman, S. (2015). Transcriptome-wide RNA processing kinetics revealed using extremely short 4tU labeling. *Genome Biol.* *16*, 282.
- Batisse, J., Batisse, C., Budd, A., Böttcher, B., and Hurt, E. (2009). Purification of nuclear poly(A)-binding protein Nab2 reveals association with the yeast transcriptome and a messenger ribonucleoprotein core structure. *J. Biol. Chem.* *284*, 34911–34917.
- Bossie, M.A., DeHoratius, C., Barcelo, G., and Silver, P. (1992). A mutant nuclear protein with similarity to RNA binding proteins interferes with nuclear import in yeast. *Mol. Biol. Cell* *3*, 875–893.
- Bresson, S., Tuck, A., Staneva, D., and Tollervey, D. (2017). Nuclear RNA decay pathways aid rapid remodeling of gene expression in yeast. *Mol. Cell* *65*, 787–800.e5.
- Castells-Roca, L., García-Martínez, J., Moreno, J., Herrero, E., Bellí, G., and Pérez-Ortín, J.E. (2011). Heat shock response in yeast involves changes in both transcription rates and mRNA stabilities. *PLoS ONE* *6*, e17272.
- Churchman, L.S., and Weissman, J.S. (2011). Nascent transcript sequencing visualizes transcription at nucleotide resolution. *Nature* *469*, 368–373.
- Dobin, A., Davis, C.A., Schlesinger, F., Drenkow, J., Zaleski, C., Jha, S., Batut, P., Chaisson, M., and Gingeras, T.R. (2013). STAR: ultrafast universal RNA-seq aligner. *Bioinformatics* *29*, 15–21.
- Doye, V., Wepf, R., and Hurt, E.C. (1994). A novel nuclear pore protein Nup133p with distinct roles in poly(A)⁺ RNA transport and nuclear pore distribution. *EMBO J.* *13*, 6062–6075.
- Gilbert, W., and Guthrie, C. (2004). The Glc7p nuclear phosphatase promotes mRNA export by facilitating association of Mex67p with mRNA. *Mol. Cell* *13*, 201–212.
- Gorsch, L.C., Dockendorff, T.C., and Cole, C.N. (1995). A conditional allele of the novel repeat-containing yeast nucleoporin RAT7/NUP159 causes both rapid cessation of mRNA export and reversible clustering of nuclear pore complexes. *J. Cell Biol.* *129*, 939–955.
- Grant, R.P., Marshall, N.J., Yang, J.C., Fasken, M.B., Kelly, S.M., Harreman, M.T., Neuhaus, D., Corbett, A.H., and Stewart, M. (2008). Structure of the N-terminal Mlp1-binding domain of the *Saccharomyces cerevisiae* mRNA-binding protein, Nab2. *J. Mol. Biol.* *376*, 1048–1059.
- Green, D.M., Marfatia, K.A., Crafton, E.B., Zhang, X., Cheng, X., and Corbett, A.H. (2002). Nab2p is required for poly(A) RNA export in *Saccharomyces cerevisiae* and is regulated by arginine methylation via Hmt1p. *J. Biol. Chem.* *277*, 7752–7760.
- Hammell, C.M., Gross, S., Zenklusen, D., Heath, C.V., Stutz, F., Moore, C., and Cole, C.N. (2002). Coupling of termination, 3' processing, and mRNA export. *Mol. Cell Biol.* *22*, 6441–6457.
- Haruki, H., Nishikawa, J., and Laemmli, U.K. (2008). The anchor-away technique: rapid, conditional establishment of yeast mutant phenotypes. *Mol. Cell* *31*, 925–932.
- Hautbergue, G.M., Hung, M.L., Golovanov, A.P., Lian, L.Y., and Wilson, S.A. (2008). Mutually exclusive interactions drive handover of mRNA from export adaptors to TAP. *Proc. Natl. Acad. Sci. U S A* *105*, 5154–5159.
- Hector, R.E., Nykamp, K.R., Dheur, S., Anderson, J.T., Non, P.J., Urbinati, C.R., Wilson, S.M., Minvielle-Sebastia, L., and Swanson, M.S. (2002). Dual requirement for yeast hnRNP Nab2p in mRNA poly(A) tail length control and nuclear export. *EMBO J.* *21*, 1800–1810.

- Hodge, C.A., Colot, H.V., Stafford, P., and Cole, C.N. (1999). Rat8p/Dbp5p is a shuttling transport factor that interacts with Rat7p/Nup159p and Gle1p and suppresses the mRNA export defect of xpo1-1 cells. *EMBO J.* **18**, 5778–5788.
- lasillo, C., Schmid, M., Yahia, Y., Maqbool, M.A., Descostes, N., Karadoulama, E., Bertrand, E., Andrau, J.C., and Jensen, T.H. (2017). ARS2 is a general suppressor of pervasive transcription. *Nucleic Acids Res.* **45**, 10229–10241.
- Iglesias, N., Tutucci, E., Gwizdek, C., Vinciguerra, P., Von Dach, E., Corbett, A.H., Dargemont, C., and Stutz, F. (2010). Ubiquitin-mediated mRNP dynamics and surveillance prior to budding yeast mRNA export. *Genes Dev.* **24**, 1927–1938.
- Jimeno, S., Rondón, A.G., Luna, R., and Aguilera, A. (2002). The yeast THO complex and mRNA export factors link RNA metabolism with transcription and genome instability. *EMBO J.* **21**, 3526–3535.
- Kelly, S.M., and Corbett, A.H. (2009). Messenger RNA export from the nucleus: a series of molecular wardrobe changes. *Traffic* **10**, 1199–1208.
- Kelly, S.M., Pabit, S.A., Kitchen, C.M., Guo, P., Marfatia, K.A., Murphy, T.J., Corbett, A.H., and Berland, K.M. (2007). Recognition of polyadenosine RNA by zinc finger proteins. *Proc. Natl. Acad. Sci. U S A* **104**, 12306–12311.
- Li, H., Handsaker, B., Wysoker, A., Fennell, T., Ruan, J., Homer, N., Marth, G., Abecasis, G., and Durbin, R.; 1000 Genome Project Data Processing Subgroup (2009). The Sequence Alignment/Map format and SAMtools. *Bioinformatics* **25**, 2078–2079.
- Libri, D., Dower, K., Boulay, J., Thomsen, R., Rosbash, M., and Jensen, T.H. (2002). Interactions between mRNA export commitment, 3'-end quality control, and nuclear degradation. *Mol. Cell. Biol.* **22**, 8254–8266.
- Love, M.I., Huber, W., and Anders, S. (2014). Moderated estimation of fold change and dispersion for RNA-seq data with DESeq2. *Genome Biol.* **15**, 550.
- Lund, M.K., and Guthrie, C. (2005). The DEAD-box protein Dbp5p is required to dissociate Mex67p from exported mRNPs at the nuclear rim. *Mol. Cell* **20**, 645–651.
- Marfatia, K.A., Crafton, E.B., Green, D.M., and Corbett, A.H. (2003). Domain analysis of the *Saccharomyces cerevisiae* heterogeneous nuclear ribonucleoprotein, Nab2p. Dissecting the requirements for Nab2p-facilitated poly(A) RNA export. *J. Biol. Chem.* **278**, 6731–6740.
- Mayer, A., Lidschreiber, M., Siebert, M., Leike, K., Söding, J., and Cramer, P. (2010). Uniform transitions of the general RNA polymerase II transcription complex. *Nat. Struct. Mol. Biol.* **17**, 1272–1278.
- Miller, C., Schwalb, B., Maier, K., Schulz, D., Dümcke, S., Zacher, B., Mayer, A., Sydow, J., Marciniowski, L., Dölken, L., et al. (2011). Dynamic transcriptome analysis measures rates of mRNA synthesis and decay in yeast. *Mol. Syst. Biol.* **7**, 458.
- Milligan, L., Huynh-Thu, V.A., Delan-Forino, C., Tuck, A., Petfalski, E., Lombrana, R., Sanguinetti, G., Kudla, G., and Tollervey, D. (2016). Strand-specific, high-resolution mapping of modified RNA polymerase II. *Mol. Syst. Biol.* **12**, 874.
- Minvielle-Sebastia, L., Winsor, B., Bonneaud, N., and Lacroute, F. (1991). Mutations in the yeast RNA14 and RNA15 genes result in an abnormal mRNA decay rate; sequence analysis reveals an RNA-binding domain in the RNA15 protein. *Mol. Cell. Biol.* **11**, 3075–3087.
- Morawska, M., and Ulrich, H.D. (2013). An expanded tool kit for the auxin-inducible degron system in budding yeast. *Yeast* **30**, 341–351.
- Parker, R. (2012). RNA degradation in *Saccharomyces cerevisiae*. *Genetics* **191**, 671–702.
- Porrua, O., and Libri, D. (2015). Transcription termination and the control of the transcriptome: why, where and how to stop. *Nat. Rev. Mol. Cell Biol.* **16**, 190–202.
- Portman, D.S., O'Connor, J.P., and Dreyfuss, G. (1997). YRA1, an essential *Saccharomyces cerevisiae* gene, encodes a novel nuclear protein with RNA annealing activity. *RNA* **3**, 527–537.
- Presnyak, V., Alhusaini, N., Chen, Y.H., Martin, S., Morris, N., Kline, N., Olson, S., Weinberg, D., Baker, K.E., Graveley, B.R., and Collier, J. (2015). Codon optimality is a major determinant of mRNA stability. *Cell* **160**, 1111–1124.
- Ramírez, F., Ryan, D.P., Grüning, B., Bhardwaj, V., Kilpert, F., Richter, A.S., Heyne, S., Dündar, F., and Manke, T. (2016). deepTools2: a next generation web server for deep-sequencing data analysis. *Nucleic Acids Res.* **44** (W1), W160–W165.
- Roth, K.M., Byam, J., Fang, F., and Butler, J.S. (2009). Regulation of NAB2 mRNA 3'-end formation requires the core exosome and the Trf4p component of the TRAMP complex. *RNA* **15**, 1045–1058.
- Rougemaille, M., Gudipati, R.K., Olesen, J.R., Thomsen, R., Seraphin, B., Libri, D., and Jensen, T.H. (2007). Dissecting mechanisms of nuclear mRNA surveillance in THO/sub2 complex mutants. *EMBO J.* **26**, 2317–2326.
- Roy, K., and Chanfreau, G. (2014). Stress-induced nuclear RNA degradation pathways regulate yeast bromodomain factor 2 to promote cell survival. *PLoS Genet.* **10**, e1004661.
- Santos-Rosa, H., Moreno, H., Simos, G., Segref, A., Fahrenkrog, B., Panté, N., and Hurt, E. (1998). Nuclear mRNA export requires complex formation between Mex67p and Mtr2p at the nuclear pores. *Mol. Cell. Biol.* **18**, 6826–6838.
- Schmid, M., Olszewski, P., Pelechano, V., Gupta, I., Steinmetz, L.M., and Jensen, T.H. (2015). The nuclear polyA-binding protein Nab2p is essential for mRNA production. *Cell Rep.* **12**, 128–139.
- Schmid, M., Tudek, A., and Jensen, T.H. (2018). Simultaneous Measurement of Transcriptional and Post-transcriptional Parameters by 3'-end RNA-seq. *Cell Rep.* **24**, this issue, 2468–2478.
- Segref, A., Sharma, K., Doye, V., Hellwig, A., Huber, J., Lührmann, R., and Hurt, E. (1997). Mex67p, a novel factor for nuclear mRNA export, binds to both poly(A)+ RNA and nuclear pores. *EMBO J.* **16**, 3256–3271.
- Strahm, Y., Fahrenkrog, B., Zenklusen, D., Rychner, E., Kantor, J., Rosbach, M., and Stutz, F. (1999). The RNA export factor Gle1p is located on the cytoplasmic fibrils of the NPC and physically interacts with the FG-nucleoporin Rip1p, the DEAD-box protein Rat8p/Dbp5p and a new protein Ymr 255p. *EMBO J.* **18**, 5761–5777.
- Strambio-de-Castilla, C., Blobel, G., and Rout, M.P. (1999). Proteins connecting the nuclear pore complex with the nuclear interior. *J. Cell Biol.* **144**, 839–855.
- Sun, M., Schwalb, B., Schulz, D., Pirkl, N., Etzold, S., Larivière, L., Maier, K.C., Seizl, M., Tresch, A., and Cramer, P. (2012). Comparative dynamic transcriptome analysis (cDTA) reveals mutual feedback between mRNA synthesis and degradation. *Genome Res.* **22**, 1350–1359.
- Terry, L.J., and Wenthe, S.R. (2007). Nuclear mRNA export requires specific FG nucleoporins for translocation through the nuclear pore complex. *J. Cell Biol.* **178**, 1121–1132.
- Thomsen, R., Nielsen, P.S., and Jensen, T.H. (2005). Dramatically improved RNA in situ hybridization signals using LNA-modified probes. *RNA* **11**, 1745–1748.
- Tran, E.J., Zhou, Y., Corbett, A.H., and Wenthe, S.R. (2007). The DEAD-box protein Dbp5 controls mRNA export by triggering specific RNA:protein remodeling events. *Mol. Cell* **28**, 850–859.
- van Dijk, E.L., Chen, C.L., d'Aubenton-Carafa, Y., Gourvenec, S., Kwapisz, M., Roche, V., Bertrand, C., Silvain, M., Legoix-Né, P., Loeillet, S., et al. (2011). XUTs are a class of Xrn1-sensitive antisense regulatory non-coding RNA in yeast. *Nature* **475**, 114–117.
- Vasiljeva, L., and Buratowski, S. (2006). Nrd1 interacts with the nuclear exosome for 3' processing of RNA polymerase II transcripts. *Mol. Cell* **21**, 239–248.
- Warfield, L., Ramachandran, S., Baptista, T., Devys, D., Tora, L., and Hahn, S. (2017). Transcription of nearly all yeast RNA polymerase II-transcribed genes is dependent on transcription factor TFIIID. *Mol. Cell* **68**, 118–129.e5.
- Wery, M., Descrimes, M., Vogt, N., Dallongeville, A.S., Gautheret, D., and Morillon, A. (2016). Nonsense-mediated decay restricts LncRNA levels in

yeast unless blocked by double-stranded RNA structure. *Mol. Cell* 61, 379–392.

Wyers, F., Rougemaille, M., Badis, G., Rousselle, J.C., Dufour, M.E., Boulay, J., Régnault, B., Devaux, F., Namane, A., Séraphin, B., et al. (2005). Cryptic pol II transcripts are degraded by a nuclear quality control pathway involving a new poly(A) polymerase. *Cell* 121, 725–737.

Xu, Z., Wei, W., Gagneur, J., Perocchi, F., Clauder-Münster, S., Camblong, J., Guffanti, E., Stutz, F., Huber, W., and Steinmetz, L.M. (2009). Bidirectional promoters generate pervasive transcription in yeast. *Nature* 457, 1033–1037.

Yao, W., Roser, D., Köhler, A., Bradatsch, B., Bassler, J., and Hurt, E. (2007). Nuclear export of ribosomal 60S subunits by the general mRNA export receptor Mex67-Mtr2. *Mol. Cell* 26, 51–62.

STAR★METHODS

KEY RESOURCES TABLE

REAGENT or RESOURCE	SOURCE	IDENTIFIER
Antibodies		
anti-Rpb3p	Abcam	1Y26 cat. no.: ab81859; RRID: AB_1658381
anti-Nab2p	Hector et al., 2002	3F2
Alexa Fluor 488-labeled goat anti-mouse IgG	Invitrogen	Cat. no.: A32723; RRID: AB_2633275
anti-Pab1 1G1	Santa Cruz	Cat. no.: sc57953; RRID: AB_672248
anti-Rrp6	Jensen group	Production bleed AAU1
Chemicals, Peptides, and Recombinant Proteins		
Auxin (Indole-3-acetic acid sodium salt)	Sigma Aldrich	Cat. no.: 15148-10G
MTSEA-biotin	Biotium	Cat. no.: 90064
ProlongGold with DAPI solution	Life Technologies	Cat. no.: P36935
Rapamycin	Cayman chemicals	Cat. no.: 13346
4tU	Aldrich	Cat. no.: 440736-1G
Critical Commercial Assays		
Turbo DNase free kit	Ambion	Cat. no.: AM1907M
SuperScript II	Invitrogen	Cat. no.: 18064-014
Platinum SYBR Green qPCR Super-Mix-UDG kit	Invitrogen	Cat. no.: 11733-046
<i>Escherichia coli</i> poly(A) polymerase kit	ThermoFisher	Cat. no.: AM1350
PureLink micro RNA purification kit	Ambion	Cat. no.: 12183018A
Ribo-Zero Gold rRNA Removal kit for yeast	Illumina	Cat. No.: MRZY1306
RiboLock Rnase Inhibitor	ThermoScientific	Cat. no.: E00381
Lexogen QuantSeq 3' mRNA-Seq Library Prep Kit REV	Lexogen	Cat. no.: 016.96
RNase A/T1	Thermo Scientific	Cat. no. EN0551
PNK enzyme with buffer A	Thermo Scientific	Cat. no.: EK0031
Deposited Data		
10 min 4tU	This study	GEO: GSE108477
2 min 4tU	This study	GEO: GSE108550
Raw data for all figures	This study	www.mendeley.com at: https://doi.org/10.17632/jxw2cmh8kp.1
Experimental Models: Organisms/Strains		
<i>S. cerevisiae</i> genome	N/A	UCSC: sacCer3
<i>S. pombe</i> genome	N/A	ENSEMBL: EF2
as W303, <i>tor1-1 fpr1::loxP-LEU2-loxP RPL13-2xFKBP12::loxP-TRP1-loxP</i>	Haruki et al., 2008; Euroscarf	AA WT (HHY212)
as W303, <i>tor1-1 fpr1::loxP-LEU2-loxP PMA1-2xFKBP12::loxP-TRP1-loxP Dbp5p::FRB::HIS3</i>	This study	<i>Dbp5-AA</i>
as W303, <i>tor1-1 fpr1::NAT RPL13-2xFKBP12::TRP1 MEX67-FRB::kanMX6</i>	Haruki et al., 2008; Euroscarf	<i>Mex67-AA</i> (HHY182)
as W303, <i>tor1-1 fpr1::NAT RPL13-2xFKBP12::TRP1 MEX67-FRB::kanMX6 NAB2::FRB::HIS3</i>	This study	<i>Mex67-AA Nab2-AA</i>
as W303, <i>tor1-1 fpr1::NAT RPL13-2xFKBP12::TRP1 MEX67-FRB::kanMX6, RRP6::URA3</i>	This study	<i>Mex67-AA rrp6Δ</i>

(Continued on next page)

Continued

REAGENT or RESOURCE	SOURCE	IDENTIFIER
as W303, <i>tor1-1 fpr1::loxP-LEU-loxP RPL13-2xFKBP12::TRP1 Mtr2p-FRB::HIS3</i>	This study	<i>Mtr2-AA</i>
as W303, <i>tor1-1 fpr1::loxP-LEU-loxP RPL13-2xFKBP12::TRP1 Nab2p-FRB::HIS3</i>	Schmid et al., 2015	<i>Nab2-AA</i>
as W303, <i>tor1-1 fpr1::loxP-LEU-loxP Pma1::FKBP::TRP1 Npl3p::FRB::GFP::HIS3</i>	This study	<i>Npl3-AA</i>
as W303, <i>tor1-1 fpr1::LEU RPL13-2xFKBP12::loxP-TRP1-loxP, OsTIR::URA, RAT1::AID::KanMX, Mex67::FRB::KanMX</i>	This study	<i>Rat1-AID Mex67-AA</i>
as W303, <i>tor1-1 fpr1::LEU RPL13-2xFKBP12::loxP-TRP1-loxP, OsTIR::URA, RAT1::AID::KanMX, XRN1::AID::KanMX, MEX67::FRB::KanMX</i>	This study	<i>Rat1-AID Xrn1-AID Mex67-AA</i>
As W303, <i>tor1-1, fpr1::loxP-LEU2-loxP, RPL13-2xFKBP12::loxP-TRP1-loxP, RRP6-FRB::HIS3, DIS3-FRB::KAN</i>	This study	<i>Rrp6-AA Dis3-AA</i>
As W303, <i>tor1-1 fpr1::LEU, RPL13-2xFKBP12::loxP-TRP1-loxP, DIS3::FRB::KanMX, RRP6::FRB::HIS, mex67-5i</i>	This study	<i>Rrp6-AA Dis3-AA mex67-5i</i>
as W303, <i>tor1-1 fpr1::loxP-LEU-loxP RPL13-2xFKBP12::TRP1 Yra1p-FRB::HIS3</i>	This study	<i>Yra1-AA</i>
<i>leu2-3,112 trp1-1 can1-100 ura3-1 ade2-1 his3-11,15</i>		WT W303
as W303, <i>MATa, gle1Δ::HIS3 < gle1-37, leu2, cen ></i>	Strahm et al., 1999	<i>gle1-37</i>
as W303, <i>MATa, mex67-5</i>	Jimeno et al., 2002	<i>mex67-5i</i>
as W303, <i>mlp1Δ::URA3</i>	Strambio-de-Castillia et al., 1999	<i>mlp1Δ</i>
as W303, <i>mlp2Δ::HIS33</i>	Strambio-de-Castillia et al., 1999	<i>mlp2Δ</i>
as BY, <i>MATalpha, his3Δ1, leu2Δ0, lys2Δ0 ura3Δ0W303, MATalpha, nup60Δ::KanMX6</i>	Lund and Guthrie, 2005	<i>nup60Δ</i>
as W303, <i>MATa, nup116-5::HIS3</i>	Terry and Wentle, 2007	<i>nup116Δ</i>
as W303, <i>MATalpha, nup133::HIS3</i>	Doye et al., 1994	<i>nup133Δ</i>
as W303, <i>rat7-1, trp1Δ63, ura3-52, leu2Δ1</i>	Gorsch et al., 1995	<i>rat1-7 (nup159 mut)</i>
Oligonucleotides		
See Table S3 in Supplemental Information	N/A	N/A
Recombinant DNA		
2μ, ori(f1), ori(pMB1), URA3, Amp ^r , LacZ, MCS, T7 promoter, T3 promoter	ATCC 77107	pRS426
2μ, ori(f1), ori(pMB1), URA3, Amp ^r , LacZ, MCS, T7 promoter, T3 promoter, NAB2 in KpnI-XhoI	PAC717 kind gift from A. Corbett	pRS246-NAB2
2μ, ori(f1), ori(pMB1), URA3, Amp ^r , LacZ, MCS, T7 promoter, T3 promoter, FUI1	Barrass et al., 2015	p4FUI(URA)
2μ, ori(f1), ori(pUC), URA3, Amp ^r , T _{CYC1} , MCS, P _{GAL1} , P _{GAL10} , MCS, T _{ADH1}	Stratagene	pESC_URA
2μ, ori(f1), ori(pUC), URA3, Amp ^r , T _{CYC1} , MCS, P _{GAL1} , P _{GAL10} , NAB2 ORF, T _{ADH1}	This work	pPgal_Nab2
Software and Algorithms		
ImageJ	https://imagej.nih.gov/ij/	N/A
DAPI area selection macro for ImageJ	This study	N/A
BBMAP v 35.92	https://jgi.doe.gov/data-and-tools/bbtools/	unpublished
STAR aligner v GitHub 2016-03-14	https://github.com/alexdobin/STAR	Dobin et al., 2013
samtools v 1.3	http://www.htslib.org/	Li et al., 2009
HTSeq v 0.6.0	https://pypi.python.org/pypi/HTSeq	Anders et al., 2015
R package DESeq2 v 1.10.1	http://bioconductor.org/packages/release/bioc/html/DESeq2.html	Love et al., 2014

(Continued on next page)

Continued		
REAGENT or RESOURCE	SOURCE	IDENTIFIER
deepTools2 software suite v2.2.4	http://deeptools.readthedocs.io/en/latest/index.html	Ramírez et al., 2016
GitHub	https://github.com/manschmi/MexNab_3seq	N/A
Other		
Aria MX Real Time PCR System	Agilent Technologies	Cat. no.: G8830A
Axiovert 200M microscope Cy3, DAPI, FITC filters	Zeiss	N/A
Covaris S2 Focused Ultrasonicator	Covaris	N/A
Bioanalyzer	Agilent	N/A
Dynabeads M280 Sheep anti-mouse IgG	Invitrogen	Cat. no.: 11202D
Dynabeads MyOne Streptavidin C1	Invitrogen	Cat. no.: 65002
MG-SR PLUS X-ray films	Konica Minolta	Cat. no.: A3WM
NuPAGE 4-12% Bis-Tris Protein Gels	ThermoFisher Scientific	Cat. no.: NP0322BOX
NuPage 4x loading dye	Thermo Fisher	Cat. no. NP0007
Typhoon FLA9500	GeHealthcare	Cat. no.: 28996943
UV Stratalinker 1800	Stratagene	N/A
Zeba Spin Desalting Columns 7KMWCO	Thermo Scientific	Cat. no.: 89890
3-8% Tris acetate gel	Invitrogen	Cat. no.: EA03755BOX
RNAPII ChIP-tiling array	Mayer et al., 2010	ArrayExpress E-TABM-1033
RNAPII ChIP-seq	Warfield et al., 2017	sample GSM2551210 from GEO:GSE97081
NETseq	Churchman and Weissman, 2011	sample GSM617027 from GEO:GSE25107
RNAPII CRAC	Milligan et al., 2016	sample GSM1706520 from GEO:GSE69676
cDTA	Sun et al., 2012	ArrayExpress: E-MTAB-760
DTA	Miller et al., 2011	ArrayExpress: E-MTAB-439
<i>rpb1-1</i> chase	Presnyak et al., 2015	GEO: GSE57385

CONTACT FOR REAGENT AND RESOURCE SHARING

Further information and requests for resources and reagents should be directed to and will be fulfilled by the Lead Contact, Torben Heick Jensen (e-mail: thj@mbg.au.dk).

EXPERIMENTAL MODEL AND SUBJECT DETAILS

Yeast strains, growth conditions and plasmids

AA strains were constructed using materials described in [Haruki et al. \(2008\)](#) and according to standard procedures. For assessment of RNA abundance and localization, cells were grown in YPAD media at 30°C. If *HSP104* and *SSA4* expression was assessed cells were pre-grown in YPAD media at 25°C and shifted to 38°C for 10-12 min by adding an equal volume of media at 51°C. To test RNA net production by 4tU labeling and perform Rpb3p and Nab2p ChIP analysis, cells were transformed with pESC_URA, pPgal_Nab2, p4FUI(URA3), pRS426(URA3) or pRS426-NAB2(URA3) plasmids and grown in minimal media lacking uracil, to increase 4tU uptake. When needed, rapamycin or auxin were added to the media to a final concentration of 1 µg/ml or 3 mM as specified in ([Haruki et al., 2008](#); [Morawska and Ulrich, 2013](#)). If needed cells were grown in 2% galactose media. Cells for RNA extraction were harvested by mixing equal volumes of culture with 96% ethanol pre-cooled on dry-ice. Yeast strains and plasmids used in this study are listed in Key Resource Table sections 'Experimental Models': 'Organisms/Strains' and 'Recombinant DNA', respectively.

METHOD DETAILS

RNA extraction, reverse-transcription and qPCR

RNAs were extracted using the hot-acid phenol method. Briefly cell pellets were suspended in TES buffer (1% SDS, 5 mM EDTA, 10 mM Tris pH 7.5) and extracted twice with phenol at 65°C with shaking for 30 min and once in chloroform at RT for 5 min. Between washes, samples were centrifuged for 10 min at 16 000 g at 4°C. RNAs were precipitated with ethanol in 20–30 mM LiCl and resuspended in deionized water. Depending on the experiment, 200 ng to 1.5 µg of RNA was selected for DNase treatment using Invitrogen TURBO DNA-free Kit (AM1907M) according to the manufacturer's recommendation. RNAs were then reverse transcribed using a 100 µM dT18 oligonucleotide with 250 ng/µl random hexamers (Invitrogen, 48190-011) and Invitrogen SuperScript II (18064-014) kit according to the manufacturer's recommendation. qPCR reactions were prepared using the Invitrogen Platinum SYBR Green qPCR Super-Mix-UDG (11733-046) kit and run on Aria MX Real Time PCR System from Agilent Technologies. Oligonucleotides used are listed in [Table S3](#) in [Supplemental Information](#).

ChIP of Nab2p and Rpb3p

Chromatin from Mex67-AA cells was prepared according to standard procedures. Briefly 50 mL of cells at $OD_{600} = 0.4$ – 0.6 were crosslinked with 1% final paraformaldehyde for 15 min and washed twice with 25 mL of 150 mM NaCl, 10 mM Tris-HCl pH 7.5. After washing, cells were resuspended in 1 mL of FA buffer (50 mL HEPES pH 7.5, 150 mL NaCl, 1 mL EDTA, 1% Triton X-100, 0.1% SDS, 1% Na-deoxycholate) with cComplete, Mini, EDTA-free Protease Inhibitor Cocktail (04693159001, Roche), supplemented with 0.5 mL of glass beads and vortexed for 20 min at 4°C. Chromatin was fragmented using a Covaris S2 Focused Ultrasonicator (program: 15x freq. Sweeping/duration 30 s, intensity 8.0, cycles/burst 200) and centrifuged for 25 min at 16000 g. 200 µL of the supernatant was taken for IP, which was performed with 30 µL of blocked and pre-washed in FA + 1% BSA buffer Dynabeads M280 Sheep anti-mouse IgG from Invitrogen (11202D) containing immobilized anti-Rpb3p antibody 1Y26 (Abcam, ab202893) or anti-Nab2p 3F2 ([Hector et al., 2002](#)). In order to determine the background of the IP for each condition a mock IP was performed in which the sonicated chromatin was incubated with beads not conjugated to the antibodies. After 1h30 min of incubation with the antibody-conjugated beads the resin was washed four times with 0.5 mL of FA buffer, two times with 0.5 mL of FA buffer containing 0.5 M NaCl and one time with TE (10 mM Tris-HCl pH 8.0, 1 mM EDTA pH 8.0). Precipitated chromatin was eluted for 10 min at 65°C with 100 µL of TE with 1% SDS. The elution and 10 µL of the input were treated with 5 µL of 20 mg/ml proteinase K for 30 min at 37°C and DNA fragments were purified using QIAquick PCR purification kit (28106; QIAGEN) according to manufacturer's instructions, resuspended in 0.2 mL of water and used for real-time PCR. Elutions were normalized to average of input levels. To accurately define the Nab2p/Rpb3p ratio, background was subtracted from raw values.

Nab2p RNA immunoprecipitation (RIP)

50 mL of Mex67-AA 0.45–0.60 OD cultures were incubated, or not, with rapamycin for 30 min at 30°C. Cells were centrifuged, resuspended in 1 mL of sterile water and spread on a 100 mm diameter Petri dish for cross-linking by a UV Stratalink (Stratagene). Petri dishes were placed on ice within 5 cm distance from the light source and set to receive 300 or 700 J/cm². Cells were then washed twice with 1 mL of sterile water and frozen on dry ice. Pellets were resuspended in 1.8 mL of lysis buffer (50 mM Tris-HCl, pH 7.4, 100 mM NaCl, 1% Igepal CA-630, 0.1% SDS, 0.5% sodium deoxycholate) and mixed with 1.5 mL of glass beads. Thereafter, cells were broken in a Precellys®24 tissue homogenizer employing five cycles of 45 s at 6500 rpm with 5 min incubation on ice in between cycles. Broken cell suspensions were recovered and 5 µL of Turbo DNase was added to each sample for 5 min at 37°C. After DNase treatment cells were centrifuged for 3 min at 3000 g to remove unbroken cells and the supernatant was spun again for 5 min at 16 000 g. The supernatant was recovered, and used for IP using sheep anti-mouse IgG magnetic beads M280 (Invitrogen cat no. 11202D), which were pre-incubated in lysis buffer for 90 min with anti-Nab2p antibody 3F2 ([Hector et al., 2002](#)) and 1% BSA. Nab2p was IP'ed at 4°C for 1 hour with constant rotation. After IP half of the bead suspension volume was resuspended in 1 mL of RNase A/T1 digestion buffer (10 mM Tris 7.5; 300 mM NaCl, 5 mM EDTA, 2 µl of RNase A/T1 (Thermo Scientific cat. no. EN0551)) and incubated for 7 min at room temperature. After this step both RNase (–) and (+) fractions were washed twice with 1 mL of high salt wash buffer (50 mM Tris-HCl, pH 7.4, 1 M NaCl, 1 mM EDTA, 1% Igepal CA-630, 0.1% SDS, 0.5% sodium deoxycholate). During the second wash, samples were incubated for 5 min with rotation. Beads were washed one more time with 1 mL of PNK labeling buffer (20 mM Tris-HCl, pH 7.4, 10 mM MgCl₂, 0.2% Tween-20) and 100 µL of beads in PNK buffer was mixed with 34 µl of NuPage loading dye (Thermo Fisher cat. no. NP0007) and this fraction was used for western blotting analysis ('elution' sample). The remaining beads were resuspended in 20 µL of enzymatic PNK suspension prepared with buffer A (Thermo Scientific, cat no. EK0031) and supplemented with gamma-ATP. Samples were incubated for 10 min at 37°C. The reaction mix was removed and beads were resuspended in 1x NuPage elution buffer and incubated for 5 min at 70°C. Samples were loaded on a 3%–8% Tris-acetate gel (Invitrogen cat. no. EA03755BOX). After electrophoresis the gel was washed 5 times with running buffer and imaged with phosphorimager screen on a Typhoon FLA9500 (GE Healthcare) and with MG-SR PLUS X-ray films (Konica Minolta cat. no. A3WM). Signals in the entire lanes of RNaseA/T1 non-treated samples were quantified using ImageJ software. The values displayed on the graph were normalized to the value of the +rapamycin and 700J/cm² sample and corrected for background.

Isolation of newly synthesized RNAs using 4tU labeling

Isolation of newly synthesized RNA using 4tU labeling was based on (Barrass et al., 2015) with several modifications. 50 mL of cells at OD₆₀₀ around 0.4–0.6 were grown in synthetic medium lacking uracil at 30°C. 4tU (Sigma, from a 100mM stock in DMSO) was added to a final concentration of 100 μM for 10 min or 2 min (depending on the experiment) with subsequent cooling of cells by pouring cultures into 50 mL of dry-ice cold ethanol. RNAs were extracted using the hot acid phenol method. All samples were prepared in triplicates and 10 min 4tU labeled *S. pombe* RNA was added for normalization to all samples (1 μg of *S. pombe* RNA per 100 μg of *S. cerevisiae* RNAs; *S. pombe* spike-in RNA comes from total RNA from cells grown exponentially in YPAD medium at 30°C and labeled with 5 mM 4tU for 10 minutes). Additionally, for both Nab2-AA and Mex67-AA series one negative control from cells that were neither labeled with 4tU nor treated with rapamycin was prepared to determine the background of the 4tU IP procedure. 250–350 μg of total RNA resuspended in 400 μL of 1 mM EDTA, 10 mM HEPES was biotinylated using 10 μL 5mg/ml MTSEA-biotin in DMF (90064; Biotium) for 30 min at 25°C. After biotinylation RNA was desalted using Zeba Spin Desalting Columns 7KMWCO (89890; Thermo Scientific) according to manufacturer's instructions. After desalting RNA was precipitated with ethanol and resuspended in water. An aliquot of RNA ('total' samples) was taken at this step and the remaining RNA was supplemented with salts to the final IP buffer composition: 10 mM Tris-HCl pH 7.0, 0.2 M NaCl, 25 mM MgCl₂, 0.1% SDS, 0.1 M NaPi pH 6.8. IP was performed using 30–50 μL (depending on the experiment) of Dynabeads MyOne Streptavidin C1 from Invitrogen (65002) pre-washed in IP buffer and blocked with 200 μL of glycogen. Following 30 min of IP reaction, the beads were washed five times with 0.4 mL of IP buffer and one time with 0.4 mL of TEN1000 (10 mM Tris-HCl pH 7.5, 0.5 mM EDTA, 1 M NaCl). RNA was eluted with 0.1 mL of 0.7 M beta-mercaptoethanol for 10 min at room temperature. Eluted RNA was precipitated with ethanol, 100 μg of glycogen and 20–30 mM final LiCl and resuspended in water. Depending on the application, RNA was subjected to sequencing library preparation or to RT-qPCR analysis (see relevant sections). In the latter case, IP values were normalized to *S. pombe* spike-in transcripts defined by amplification of cDNA of the *SpACT1* mRNA and to input RNA concentrations. Background values, derived from non-4tU-labeled and non-rapamycin treated samples, were then subtracted and final results depicted as ratios between rapamycin treated sample relative to appropriate control.

Western blotting analysis

Protein extracts were prepared by incubating 4–6 OD units of cells in 8 M urea at 80°C and subsequent disruption of cells using glass beads. Western blotting analysis was performed according to standard procedures. Antibodies used are listed in Resource Table under section Antibodies.

pA⁺ RNA FISH analysis and protein localization

IF and FISH samples were performed as previously described (Schmid et al., 2015). Briefly, cells were fixed with 4% final paraformaldehyde for 40 min and washed three times with 1.2 M sorbitol, 0.1 M K₂HPO₄. Cell walls were digested for 25 min at 30°C in 1.2 M sorbitol, 0.1 M K₂HPO₄, 28mM Beta-mercaptoethanol with zymolyase and spheroblasts were attached to PolyL-lysine coated slides and washed two times with PBS. After these common steps, slides were prepared either for FISH or IF analyses (see below).

For FISH analysis, cells were washed three times with 0.1 M K₂HPO₄, dehydrated with 80% ethanol at –20°C for at least 30 min, washed twice with 2xSSC for 5 min at 25°C and prehybridized in 50% formamide, 2xSSC for 10 min 25°C. Hybridization was performed in 50% formamide, 5 mM Na₂HPO₄, 2xSSC, 200 μg BSA with 1 ng of dT18 LNA Cy3-labeled probe (Thomsen et al., 2005) per sample for 16h at 37°C. After hybridization, slides were washed twice with 50% formamide, 2xSSC for 10 min at 37°C, once with 2xSSC, 0.1% Triton X-100 for 10 min at 25°C, twice with 1xSSC for 10 min at 25°C and twice with PBS for 5 min at 25°C. Slides were dried and mounted with ProlongGold with DAPI solution (Life Technologies, P36935). For IF analysis slides were washed once with PBS, 0.1% Triton X-100 for 5 min at 25°C, then incubated for 30 min at 25°C with PBS, 0.1% Triton X-100, 1% BSA. Nab2p detection was performed using anti-Nab2p 3F2 antibody (Hector et al., 2002) diluted 1:3000 in PBS, 0.1% Triton X-100 for 45 min at 25°C. The secondary antibody Alexa Fluor 488-labeled goat anti-mouse IgG (A32723; Invitrogen) was diluted 1:3000 in PBS, 0.1% Triton X-100 and applied to the slide for 45 min at 25°C. Between and after incubation with both antibodies, slides were washed four times for 5 min at 25°C with PBS, 0.1% Triton X-100. Slides were dried and mounted with ProlongGold with DAPI solution. Detection of Npl3p-GFP-FRB (Npl3-AA) was performed in live cells stained with DAPI.

FISH and IF microscopy pictures were acquired using an Axiovert 200M Zeiss microscope under 63x objective using DAPI, Cy3 or FITC filters. Each FISH picture contained a fixed number of stacks (which varied between experiments but was never smaller than 8) of 0.2 μm combined using maximum intensity projection. In order to quantify the nuclear RNA pA⁺ signal by FISH, cell nuclei were selected using DAPI images and the following macro in ImageJ: [run("Subtract Background...", "rolling=50 sliding"); setOption("BlackBackground," false); run("Make Binary"); run("Erode"); run("Dilate"); run("Analyze Particles...", "size=80-400 add"); roiManager("Show All with labels"); roiManager("Show All");]. Average nuclear RNA pA⁺ signal was calculated by dividing the Raw Integrated Density in the nuclear area and subsequently subtracting the value of the minimal pixel (giving a conservative estimate of local background and cytoplasmic signal). Cy3 and FITC channel images were aligned to a common display range (defined as the lowest and highest pixel value for all selected images) to enable comparison between images. Images of DAPI stain were background subtracted in ImageJ (settings: Rolling ball radius 50.0 pixels; sliding paraboloid).

pA⁺ RNA 3' end sequencing and bioinformatics analysis

RNA quality of total and purified 4tU labeled RNA was tested and quantified using a Bioanalyzer (Agilent). Depending on the sample 200–350 ng of RNA was used to prepare libraries. To generate pA⁻ data, an aliquot of the 2 min 4tU labeled RNAs was *in vitro* polyadenylated using *Escherichia coli* poly(A) polymerase (AM1350; ThermoFisher) according to the manufacturer's instructions. Reactions were then purified using PureLink micro RNA purification kit from Ambion (12183018A) and ribo-depleted using Ribo-Zero Gold rRNA Removal kit for yeast (MRZY1306) from Illumina according to the manufacturer's instructions. All libraries were then prepared using Lexogen QuantSeq 3' mRNA-Seq Library Prep Kit REV (016.96, Lexogen GmbH) for Illumina and sequenced at Vienna Bio-center Core Facilities (Vienna, Austria) multiplexing 32 samples on a HiSeqV4 SR50 (single end 50nt reads) run and using the QuantSeq REV specific primer CSP. An overview of samples, read quality control and mapping statistics are provided in [Table S1](#) and [Table S2](#).

Bioinformatics

Details concerning RNaseq data analysis can be found in ([Schmid et al., 2018](#)). All relevant code and analysis scripts are available at GitHub (https://github.com/manschmi/MexNab_3seq).

RNA 3' end sequencing quality control, filtering, mapping and normalization

Lexogen provided barcode splitting and the final data as unmapped bam files. We then applied quality filtering, read trimming and the mapping strategy recommended for QuantSeq REV data by Lexogen and computed genomic coverage of A-addition positions, skipping A-rich positions that allow for internal priming. Raw read coverage was then normalized to the signal obtained for the *S. pombe* genome. In case of the 4tU-labeled samples, signal from the negative control was subtracted as described in ([Schmid et al., 2018](#)). To obtain an estimate pA⁻ signal at each position, we subtracted the *S. pombe* normalized pA⁺ signal from the pA⁺ and pA⁻ signal. For the 2 min 4tU IPs this was done after background subtraction.

Annotations

mRNA and SUT annotations from ([Xu et al., 2009](#)) were lifted to UCSC sacCer3. Cryptic Unstable Transcripts (CUTs) and sn/snoRNAs from ([Xu et al., 2009](#)) were excluded from analysis since the majority of produced transcripts were not polyadenylated. XUT annotations were taken from ([Wery et al., 2016](#)). *S. pombe* genome and annotations are from ENSEMBL release EF2.

Counting gene body and end signal

Gene body regions were defined from TSSs to regions 200bp upstream of TESs (TSS to TES-200bp). Gene ends were defined as regions from 200bp upstream to 200bp downstream of the annotated TES (TES \pm 200bp). Gene body regions shorter than 100bp and parts of gene body regions, which overlapped gene end regions of neighboring genes, were removed from the analysis. For XUTs, end regions overlapping end regions of transcripts from ([Xu et al., 2009](#)) were removed from the analysis. Signals within each region were counted by custom scripts using *S. pombe* normalized, background-subtracted pA⁺ or pA⁻ bedgraph track files. Distribution of signal was then analyzed using custom scripts in R.

Differential expression analysis

Comparison of log₂ FCs signals between Mex67-AA and Nab2-AA ([Figure 1](#) and [S1](#)) was based on 10 min 4tU pA⁺ samples, where the majority of all genes has signal in the labeled fraction significantly above background (see below). pA⁺ signal from gene ends (TES \pm 200bp) from raw mapped reads (i.e., before normalization to *S. pombe* reads and without background subtraction) was collected and analyzed using the R package DESeq2 (v 1.16.1). For this, *S. pombe* based size factors were derived from reads mapping to *S. pombe* transcripts (TSS to TES+300bp) counted using a custom script based on bedtools and put to the sizeFactors function from DESeq2. pA⁺ reads from gene ends were counted using the same script and differential expression between 15 min rapamycin treated samples relative to untreated samples analyzed using independent DESeq2 calculations for IP and total RNA samples with otherwise default settings. Differential enrichment of 10 min 4tU IP samples relative to the input and enrichment of IP samples relative to the negative control IP was computed using the same procedure but by combining IP and total RNA data within one DESeq2 run. Plots depicted in [Figure 1](#) show only those RNAs with significant enrichment in the control IP relative to input samples.

Comparison of log₂ FCs in gene body and gene end regions of Mex67-AA and Nab2-AA samples in [Figure 2](#) was based on the 2 min 4tU pA⁺ samples, where the enrichment in the IP relative to negative control was less pronounced. For this analysis, background-subtracted *S. pombe*-normalized 2 min 4tU IP signals were used to measure pA⁺ signal from gene ends and pA⁻ signal from gene bodies. Regions where signals were below background were given a pseudocount of 10⁻⁶ and plots depicted in [Figure 2](#) show average values from control and 15 min samples on a log-scaled y axis.

Metagene heatmaps

Heatmaps were obtained using computeMatrix, plotHeatmap functions from the deepTools2 software suite v2.2.4 together with custom python scripts ([Iasillo et al., 2017](#)). For heatmaps of log₂ FCs between two conditions, the minimum positive value within the entire matrix added as pseudocount, and used to replace zero and negative values, mean values from replicates were computed and the log₂ FC calculated between depletion and corresponding control libraries using custom python scripts and plotted using

plotHeatmap from deepTools2. Sorting according to termination defect was done using the built-in sorting of the plotHeatmap function using a matrix containing \log_2 FC values for the region 250bp downstream the TES.

Correlation between RNA net production and published transcription and decay-rate data

Transcription and decay-rates were obtained from the relevant publications listed in the 'Other' section of the [Key Resources Table](#). Half-life and decay estimates were obtained from the Supplemental Information of the relevant publications. In cases where only half-life information was provided, decay-rates were obtained using equation $k = \ln(2)/\text{half-life}$. We also included estimated decay rates derived from the comparison of 4tU- relative to total RNA-levels using the formula: Decay Rate DR = $-(1/t) * \ln(1 - \text{RNA}_{4\text{tU}} / \text{RNA}_{\text{total}})$, akin to the strategy from (Sun et al., 2012; Miller et al., 2011). $\text{RNA}_{4\text{tU}}$ and $\text{RNA}_{\text{total}}$ are the *S. pombe* normalized and, for the 4tU IP background-subtracted, pA⁺ signal from gene ends (TES \pm 200bp) from the 10 min 4tU experiment and labeling time $t = 10$ min.

QUANTIFICATION AND STATISTICAL ANALYSIS

Quantification of FISH data was performed as described in 'pA⁺ RNA FISH analysis and protein localization' section. 4tU-labeled RNAs that were analyzed by reverse-transcription and qPCR were normalized as described in the 'Isolation of newly synthesized RNAs using 4tU labeling'. When highlighted, qPCR results were analyzed using a two-tailed paired t test and p value (P) significance is defined as follows: not significant (ns) - $p > 0.05$; * - $p \leq 0.05$; ** - $p \leq 0.01$; *** - $p \leq 0.001$ and **** - $p \leq 0.0001$. Analysis of sequencing data was performed as described in the following sections: 'Bioinformatics', 'RNA 3'end sequencing quality control, filtering, mapping and normalization', 'Counting gene body and end signal', 'Differential expression analysis', 'Metagene heatmaps' and 'Correlation between RNA net production and published transcription and decay-rate data'.

DATA AND SOFTWARE AVAILABILITY

The accession number for data from 10 min 4tU labeling experiments reported in this paper is GEO: GSE108477. The accession number for data from 2 min 4tU labeling experiments reported in this paper is GEO: GSE108550. Raw non-sequencing data has been deposited with Mendeley Data at <https://doi.org/10.17632/jxw2cmh8kp.1>.

Cell Reports, Volume 24

Supplemental Information

**A Nuclear Export Block Triggers the Decay
of Newly Synthesized Polyadenylated RNA**

Agnieszka Tudek, Manfred Schmid, Marius Makaras, J. David Barrass, Jean D. Beggs, and Torben Heick Jensen

Figure S1

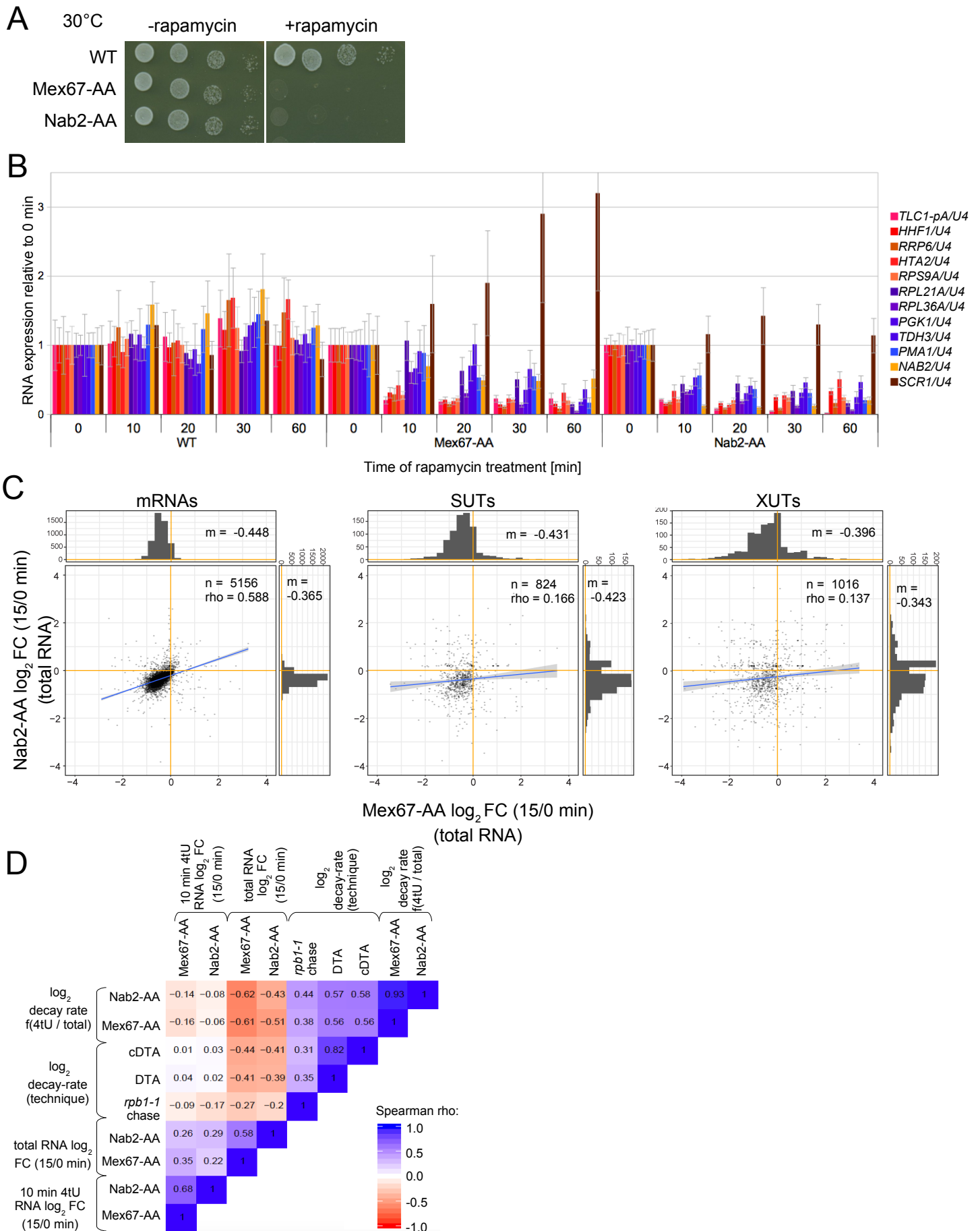


Figure S1. Related to Fig. 1

(A) Spot tests of 10x serial dilutions of WT, Mex67-AA and Nab2-AA cells plated and grown at 30°C without or with rapamycin as indicated.

(B) RT-qPCR analysis of selected RNAs, color-coded to the right of the graph, from wild-type (WT), Mex67-AA and Nab2-AA cells subjected to the indicated periods of rapamycin treatments at 30°C. RNAs that were rapidly or more slowly down-regulated in Mex67p-depleted cells are colored red and blue, respectively. Shown values were normalized to levels of *U4* RNA. *SCR1* RNA was used as a non-adenylated control. Error bars indicate standard deviations from three PCR technical replicates. The result is representative of additional biological repeats.

(C) Rapamycin-dependent changes of mRNA, SUT and XUT levels as depicted in Figure 1C, but for total RNA samples. Observed transcript changes were more modest than previously reported (Schmid et al. 2015). This is likely due to a prolonged doubling time of cells grown here in minimal media lacking uracil (to increase 4tU uptake) relative to rich media used in the previous study and in Fig. S1B. See also Table S1.

(D) Spearman correlation coefficient matrix comparing mRNA log₂FC of 15/0 min rapamycin treatment in Mex67- and Nab2-AA cells as in Fig. 1C and S1C against various estimates of decay rates. These were derived from the following published data: rpb1-1 chase experiments using total RNA (Presnyak et al., 2015), 4tU-based methods - Dynamic Transcriptome Analysis (DTA; Miller et al., 2011) and comparative DTA (cDTA; Sun et al. 2012). DRs estimated by comparing 4tU to total RNA, using established methods (Miller et al., 2011 ; Sun et al. 2012), from the data presented herein are included for comparison.

Figure S2

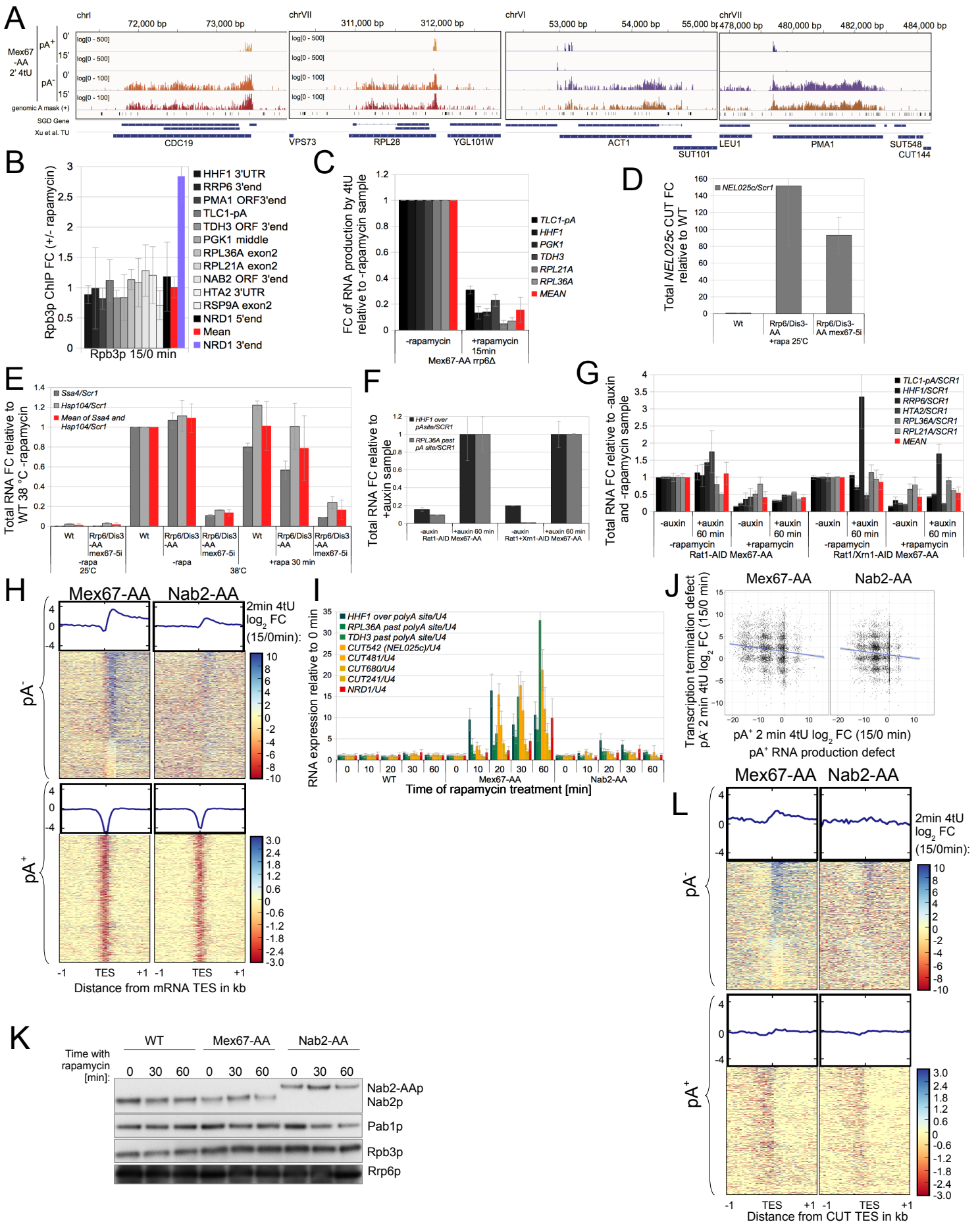
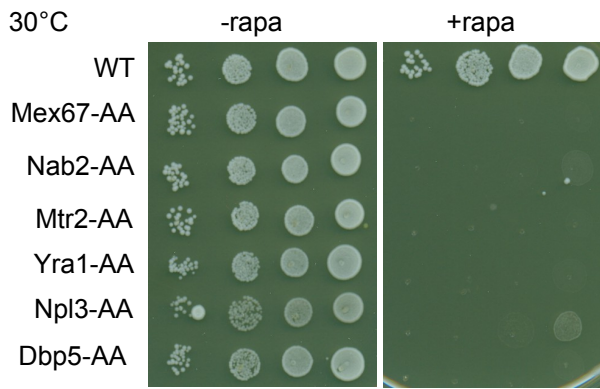


Figure S2. Related to Fig. 2.

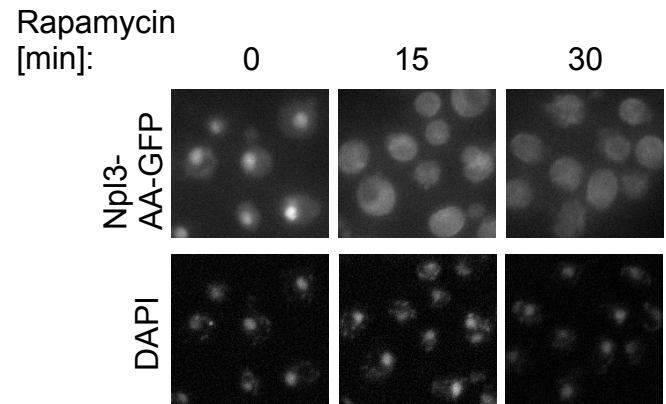
- (A)** Genome browser views of pA⁻ and pA⁺ RNA 3'end reads, derived from 2 min 4tU labeling experiments of the Mex67-AA strain, spanning across the indicated regions of chromosomes I, VI and VII. Depicted as in Fig. 2C.
- (B)** RNAPII ChIP (anti-Rpb3p) analysis of indicated genic regions in Mex67-AA cells treated for 15 min with rapamycin relative to non-rapamycin treated cells and corrected for background. Values and error bars shown for specific loci are mean RNAPII occupancies and standard deviations from three replicate IPs. Value and error bar of mean indicate mean and standard deviation of RNAPII occupancy on all tested loci from the grey series (excluding *NRD1* 3'end; blue series).
- (C)** RT-qPCR analysis of new RNAs from Mex67-AA/*rrp6*Δ cells treated with rapamycin for a total of 15 min and subjected to 10 min of 4tU-labeling. The values displayed are a mean of triplicate IPs, which were background subtracted and normalized to spike-ins and total RNA input. Values are plotted relative to the -rapamycin control. See Fig. 3C for average result in Mex67-AA *RRP6* background.
- (D)** RT-qPCR analysis of *NEL025c* CUT levels from WT, Rrp6-AA/Dis3-AA and Rrp6-AA/Dis3-AA/*mex67-5i* cells after a 30 min rapamycin treatment. Error bars represent standard deviations of PCR technical replicates from one representative experiment.
- (E)** RT-qPCR analysis of fold changes in *SSA4* and *HSP104* RNA levels in cells nuclear-depleted for 30 minutes of Rrp6p and Dis3p, and containing, or not, the *mex67-5i* mutated gene relative to a wild-type strain. Cells were incubated for 12 min at 38 °C. Shown values are means of two independent experiments and error bars represent median absolute deviation.
- (F)** RT-qPCR analysis showing levels of read-through transcripts deriving from impaired transcription termination at *HHF1* and *RPL36A* loci in Rat1-AID/Mex67-AA and Rat1-AID/Xrn1-AID/Mex67-AA cells treated, or not, with auxin for 1 hour. Values represent the means of duplicate samples prepared in parallel and error bars are median absolute deviations.
- (G)** RT-qPCR analysis of indicated transcripts from Rat1-AID/Mex67-AA and Rat1-AID/Xrn1-AID/Mex67-AA cells treated, or not, with auxin for 1 hour prior to a 15 min rapamycin exposure. Values represent means of duplicate samples prepared in parallel and error bars are median absolute deviations. The mean series represents an average of all tested transcripts. For technical reasons the *RRP6* mRNA values was excluded from the mean in Rat1-AID/Xrn1-AID Mex67-AA series.
- (H)** Heat maps and metagene analysis displaying log₂FC densities of 2 min labeled 4tU RNA 1 kb up- and downstream of protein coding TESs in the pA⁻ (top) and pA⁺ (bottom) fractions, between Mex67-AA (left) and Nab2-AA (right) cells treated with rapamycin for 15 min relative to untreated cells. Transcript orders are the same in all heat maps and based on the strength of the termination defect in the Mex67-AA strain, estimated by the total log₂FC of pA⁻ reads in the 250bp downstream the TES.
- (I)** RT-qPCR analysis of selected RNAs from WT, Mex67-AA and Nab2-AA cells subjected to the indicated periods of rapamycin treatments at 30°C. PCR amplicons spanned the regions around or past the pA sites of three mRNAs (green series), the mid regions of four CUTs (orange series) and the 5'end of the *NRD1* RNA (red bar; note a similar result was obtained using a 3'end amplicon (data not shown)) as indicated to the right of the image. Error bars indicate standard deviations from three PCR technical replicates. The result is representative of additional biological repeats.
- (J)** Scatter plot showing the relationship between the strength of the transcription termination defect (y-axis), defined as in Fig. S2H as the mean log₂FC in the region 250bp downstream the TES, and the decrease in RNA pA⁺ 3'ends (x-axis) as mean log₂FC in the region +/-50bp around the TES. Log₂FC values were derived from the 2 min 4tU labeled fractions of Mex67-AA and Nab2-AA cells treated for 15 relative to 0 min rapamycin.
- (K)** Western blotting analysis showing levels of Nab2p (endogenous or AA-tagged), Pab1p, Rpb3p and Rrp6p in the indicated strains and growth conditions.
- (L)** Heat maps and metagene analysis displaying log₂FC of 15/0 min rapamycin ratios in Mex67- (left) and Nab2-AA (right) cells of 2 min labeled 4tU RNA. Shown is the region 1 kb up- and downstream of CUT loci TESs in the pA⁻ (upper) and pA⁺ (lower) fractions. Transcript orders are the same in all heat maps and based on the strength of the termination defect in the Mex67-AA strain, estimated by the total log₂FC of pA⁻ reads in the 250bp downstream the TES.

Figure S3

A



B



C

38°C, 12 min

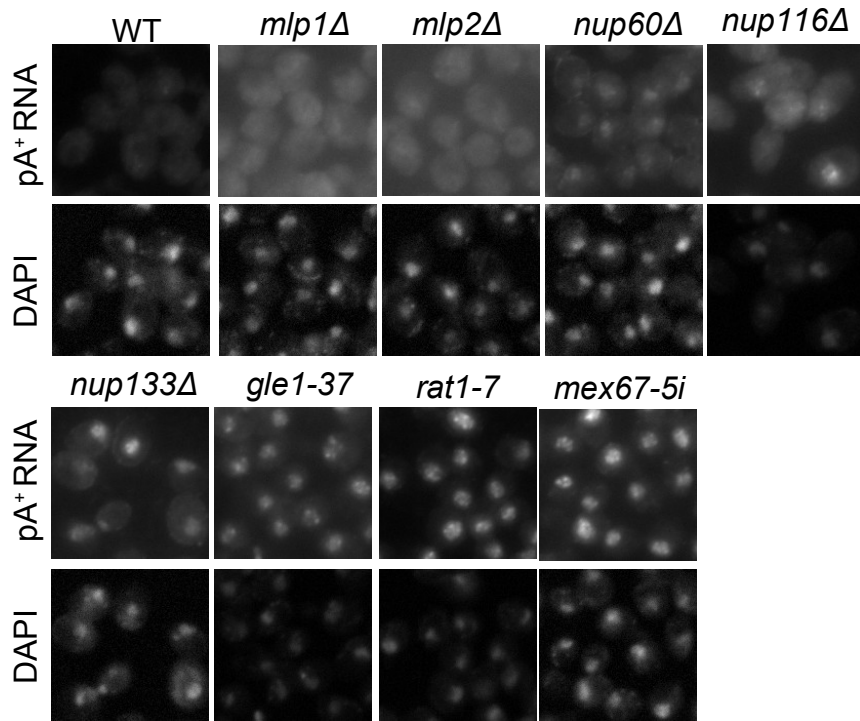


Figure S3. Related to Fig. 3.

(A) Spot tests of 10x serial dilutions of WT, Mex67-, Nab2-, Mtr2- Yra1-, Npl3- and Dbp5-AA cells plated and grown at 30°C without or with rapamycin as indicated.

(B) Sub-cellular localization of GFP-tagged Npl3-AA protein at 0, 15 and 30 min after rapamycin addition. Images were adjusted and stained with DAPI as in Fig. 1A.

(C) FISH analysis of pA+ RNA, as in Fig. 1A, on WT, *mlp1Δ*, *mlp2Δ*, *nup60Δ*, *nup116Δ*, *nup133Δ*, *gle1-37*, *rat7-1* and *mex67-5i* cells subjected to 12 min of incubation at 38°C before fixation. Note that *nup60Δ* is in the BY background as opposed to the remaining strains, which are W303. FISH images were adjusted and DAPI stained as in Fig. 1A.

Figure S4

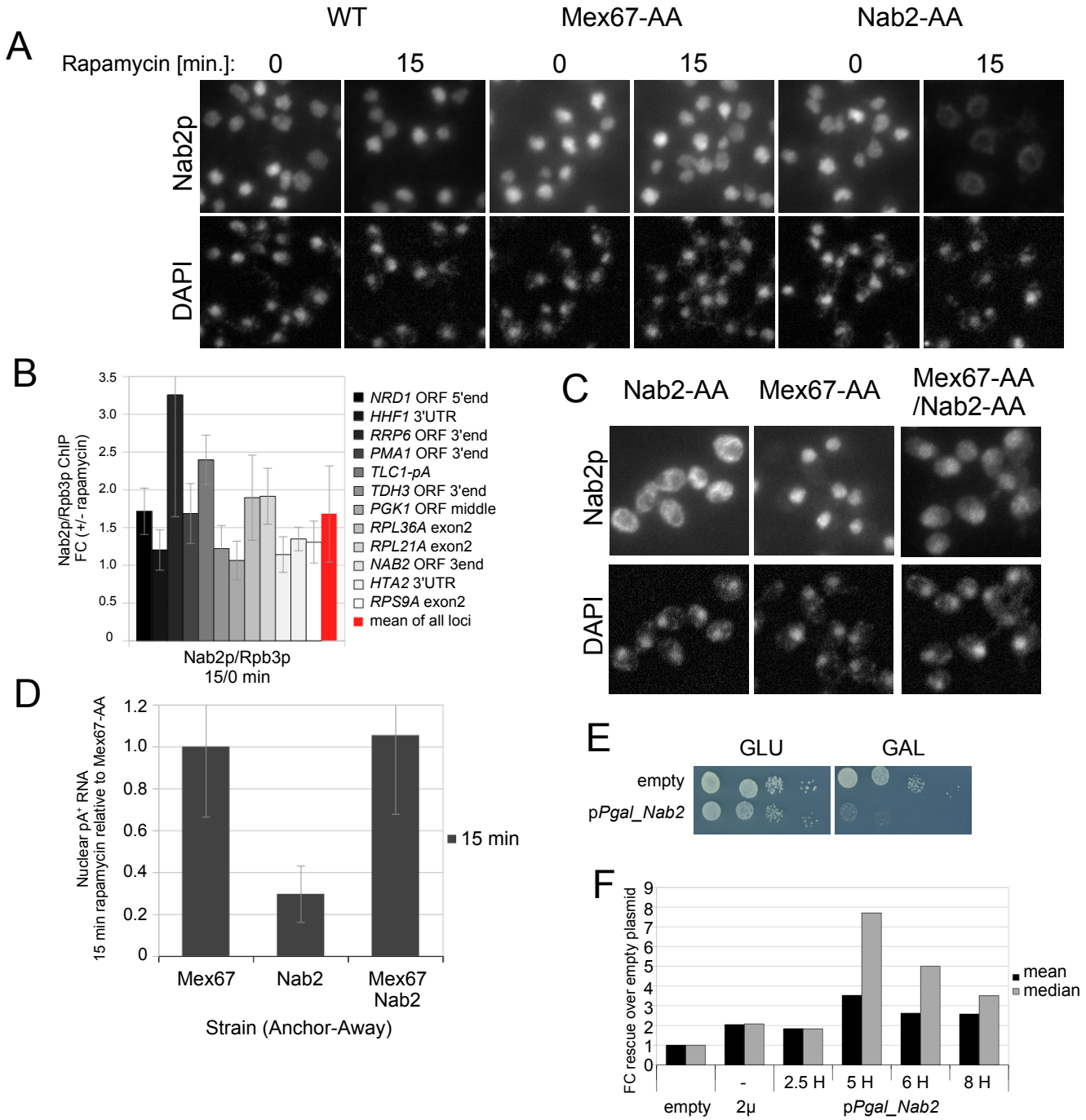


Figure S4. Related to Fig. 4.

- (A)** Immuno-localization of Nab2p without or 15 min after rapamycin treatment of WT, Mex67-AA and Nab2-AA cells as indicated. Images were adjusted and stained with DAPI as in Fig. 1A.
- (B)** ChIP of Nab2p at the indicated genic regions in Mex67-AA cells treated for 0 or 15 min with rapamycin. Values were corrected for mock IPs (no antibody) and are displayed relative to control values and normalized to Rpb3 ChIP signal. The Rpb3p levels are shown in Fig. 2D. Values and error bars shown are mean Nab2p/Rpb3 ratios and standard deviations from three replicate IPs.
- (C)** Immuno-localization of Nab2p in Nab2-, Mex67- and Nab2-/Mex67-AA cells treated with rapamycin for 15 min. Images were adjusted and stained with DAPI as in Fig. 1A.
- (D)** Quantification of nuclear pA⁺ RNA signals from AA cells employed in Fig. S4C. Values are shown relative to mean values of Mex67-AA cells and corrected for background signals. Error bars at individual time points indicate standard deviations calculated from nuclear pA⁺ RNA levels of a minimum of 1000 cells counted for each strain.
- (E)** Spot tests of 10x serial dilutions of the Mex67-AA strain containing empty or *Pgal_Nab2* plasmids on media containing glucose or galactose as indicated.
- (F)** Graph showing the mean and median fold rescue of net RNA production in Mex67-AA depletion conditions with overexpression of Nab2p, using either a 2 μ or a *pPgal_Nab2* plasmid, relative to cells containing an empty plasmid.

Table S1. Related to Figure 1. Overview of RNA-seq libraries.

Sample name (Strain_ fraction_ rapamycin[min]_ repeat)	Raw		Quality filtering	Uniquely mapped reads mapped to <i>S. cerevisiae</i> – <i>S.</i> <i>pombe</i> joint genome		Final <i>S.</i> <i>cerevisiae</i> reads after filtering for genomic A- rich positions
	Reads	Bases	Output reads	Mapped to <i>S. cerevisiae</i>	Mapped to <i>S. pombe</i>	
Nab_in_0_1	7273102	363655100	6979478	5396295	106881	4763184
Nab_in_15_1	3281586	164079300	3089524	2357069	71017	2076661
Nab_in_0_2	7891737	394586850	7538600	5482125	147565	4779771
Nab_in_15_2	7667549	383377450	7317712	5483223	133231	4762969
Nab_in_0_3	8925940	446297000	8624626	6450346	184617	5636310
Nab_in_15_3	8889698	444484900	8587558	6574692	197926	5763307
Nab_in_neg	5723825	286191250	5348882	4077028	109698	3607338
Mex_in_0_1	7452143	372607150	7052033	5942399	137163	5210550
Mex_in_15_1	7029611	351480550	6654170	5541109	176583	4851797
Mex_in_0_2	6075011	303750550	5671419	4707318	112692	4141477
Mex_in_15_2	5530398	276519900	5249025	4402660	81556	3843771
Mex_in_0_3	11875239	593761950	1,10E+007	10113976	235737	9052288
Mex_in_15_3	9698340	484917000	9247959	8171197	273885	7285130
Mex_in_neg	6039488	301974400	5824464	5261497	72637	4687659
Nab_ip_0_1	7538811	376940550	6704203	5876655	192255	5137191
Nab_ip_15_1	5565816	278290800	4908625	3924799	390638	3346347
Nab_ip_0_2	5684152	284207600	5308706	4597870	193963	3982006
Nab_ip_15_2	5152085	257604250	4487987	3665898	260786	3105436
Nab_ip_0_3	6918132	345906600	6731904	5694365	284033	4916991
Nab_ip_15_3	5857971	292898550	5234941	4191233	411475	3565773
Nab_ip_neg	9371130	468556500	8990840	5521766	1494515	4786756
Mex_ip_0_1	8246616	412330800	7843586	7150452	165124	6143287
Mex_ip_15_1	6647995	332399750	6077795	4930616	508465	3982991
Mex_ip_0_2	8144473	407223650	7785564	7054968	196736	6060297
Mex_ip_15_2	5758583	287929150	5091018	4323077	256616	3535866
Mex_ip_0_3	6176401	308820050	5675320	5173699	138931	4553450
Mex_ip_15_3	5313483	265674150	4598710	3742082	431698	3114382
Mex_ip_neg	7863817	393190850	7409785	5603811	851599	4910928

Table S2. Related to Figure 2. Overview of RNA-seq libraries.

Sample name (Papreatment_ Strain_ fraction_ rapamycin[min])_ repeat)	Raw		Quality filtering	Uniquely mapped reads mapped to <i>S. cerevisiae</i> – <i>S. pombe</i> joint genome		Final <i>S.</i> <i>cerevisiae</i> reads after filtering for genomic A- rich positions
	Reads	Bases	Output reads	Mapped to <i>S.</i> <i>cerevisiae</i>	Mapped to <i>S. pombe</i>	
noPap_Nab2AA_input_0_1	3334641	166732050	3282063	2595050	42095	2313940
noPap_Nab2AA_input_15_1	4873541	243677050	4804672	3634113	74302	3235115
noPap_Mex67AA_input_0_1	3054292	152714600	3002568	2467734	41709	2202503
noPap_Mex67AA_input_15_1	4199856	209992800	4155534	3352405	74880	2963985
noPap_Nab2AA_ip_0_1	3056716	152835800	2929431	2015728	377298	1769572
noPap_Nab2AA_ip_15_1	3666193	183309650	3552089	2195539	591965	1905171
noPap_Mex67AA_ip_neg0_1	5253477	262673850	5060704	3517377	795545	3116325
noPap_Mex67AA_ip_0_1	4038165	201908250	3883937	2949235	456822	2579454
noPap_Mex67AA_ip_15_1	2973551	148677550	2929123	2110422	519671	1837564
xPap_Nab2AA_input_0_1	5162819	258140950	4787399	3944905	40380	3822077
xPap_Nab2AA_input_15_1	4548001	227400050	4315658	3626890	35202	3530828
xPap_Mex67AA_input_0_1	4916981	245849050	4442576	3781260	35565	3654903
xPap_Mex67AA_input_15_1	6722820	336141000	6608844	5519178	59857	5390170
xPap_Nab2AA_ip_0_1	3933492	196674600	3394680	2057164	434311	1888025
xPap_Nab2AA_ip_0_2	4866432	243321600	4448755	3040507	192401	2815418
xPap_Nab2AA_ip_0_3	4189502	209475100	3675178	2446311	163220	2214857
xPap_Nab2AA_ip_15_1	5306967	265348350	4974073	2196866	138905	1901498
xPap_Nab2AA_ip_15_2	4571542	228577100	4215557	2547243	160215	2208254
xPap_Nab2AA_ip_15_3	3587820	179391000	3279510	2104394	144518	1902227
xPap_Mex67AA_ip_neg0_1	5649907	282495350	5045569	3579615	435360	3153307
xPap_Mex67AA_ip_0_1	4690443	234522150	4153541	2855569	151361	2648241
xPap_Mex67AA_ip_0_2	5035947	251797350	4645361	3156133	175134	3022976
xPap_Mex67AA_ip_0_3	3847037	192351850	3658720	2459241	132147	2310471
xPap_Mex67AA_ip_15_1	4738414	236920700	4308097	3044177	174875	2904716
xPap_Mex67AA_ip_15_2	6222728	311136400	5579940	3668144	213321	3379732
xPap_Mex67AA_ip_15_3	4208805	210440250	3326805	2260905	140711	2072147

Table S3. Related to Key Resource Table. Oligonucleotides used in this study.

Oligonucleotide name and sequence	Source	Cat. no.
Act1_S.pombe_fwd CCATTCTTGCTTCTCTTTCTACTTTCC	Sigma	custom-made
Act1_S.pombe_rev CGCTCTCATCATACTCTTGCT	Sigma	custom-made
CUT241_fwd ACCAACATAAGATATAGCTAGCAATTC	Sigma	custom-made
CUT241_rev CTCTCCAAAACAGACCAAACA	Sigma	custom-made
CUT481_fwd AGGTCAATAACGCAGACACA	Sigma	custom-made
CUT481_rev TGCTGAATCTCCAACGCT	Sigma	custom-made
CUT542 (NEL025c)_fwd ACTCTGCGATCCAAATTCTACT	Sigma	custom-made
CUT542 (NEL025c)_rev ATGCGTCTTTCCTGTTTATGAG	Sigma	custom-made
CUT680_fwd CTTTTGTTTGTGGTTGTTGTCG	Sigma	custom-made
CUT680_rev ATCGTCTTTCCTAATGGTCTTG	Sigma	custom-made
DT18 TTTTTTTTTTTTTTTTTT	Sigma	custom-made
dT18 LNA (FISH probe) TTTTTTTTTTTTTTTTTT	Thomsen et al., 2005	N/A
Hhf1_fwd ACTGCCCGTTTTTCTTCT	Sigma	custom-made
Hhf1_rev CCTAAACCCGCTATAATACACTCAT	Sigma	custom-made
Hhf1_past_polyAsite_rev TCCCTATTCCATGCAAGTTC	Sigma	custom-made
Hsp104_3'end_fwd AGCTGAAGAATGTCTGGAAGT	Sigma	custom-made
Hsp104_3'end_rev CGTCATCACCTAACGTGTCA	Sigma	custom-made
Hta2_fwd GTCATTTGGGGTTTTAAAGTAGGT	Sigma	custom-made
Hta2_rev ACCGTAAACTTGATACGTTTTTTATTTT	Sigma	custom-made
Nrd1_5'end_fwd CATAATGCAGCAGGACGACG	Sigma	custom-made
Nrd1_5'end_rev TGTGATCAAGTGCCTAAGTG	Sigma	custom-made
Nrd1_3'end_fwd AGGAGATGCCAATGGTGC	Sigma	custom-made
Nrd1_3'end_rev GGTAATGGTTGGTTGGGGG	Sigma	custom-made
Pgk1_fwd AGGTCGATGGTCAAAGG	Sigma	custom-made
Pgk1_rev CGGCAGCACGTTGT	Sigma	custom-made
Pma1_fwd TACTGTCGTCCGTGTCTGGATCT	Sigma	custom-made
Pma1_rev CCTTCATTGGCTTACCGTTCA	Sigma	custom-made
random hexamers	Invitrogen	48190-011
Rpl21A_exon2_fwd ACAGATCTCGTACACGTTACA	Sigma	custom-made
Rpl21A_exon2_rev CGACAATGTCACCAACCT	Sigma	custom-made
Rpl36A_exon2_fwd AAGGTAAGAAGGTCACTAGCA	Sigma	custom-made
Rpl36A_exon2_rev GTTGAAGCAGCACCTTT	Sigma	custom-made
Rpl36A_pastPolyAsite_fwd GCCCATGTAAGTACTGAGCTGATAG	Sigma	custom-made
Rpl36A_pastPolyAsite_rev CGGGTAACTTATATTGCTTCAG	Sigma	custom-made
Rrp6_fwd ACGGAAAAAGATGCTGTGGATT	Sigma	custom-made
Rrp6_rev CTTTTTAGCTGCCCTTGGT	Sigma	custom-made
Rrp47_fwd AACCAATTCGAGCCCTCTAT	Sigma	custom-made
Rrp47_rev CTTCTCCCTCCTTTCTTTTTTCC	Sigma	custom-made
Scr1_fwd CCCGGCTATAATAAATCGATCT	Sigma	custom-made
Scr1_rev GCTGACGCTGGATAAAACT	Sigma	custom-made
Ssa4_fwd AAATTGTACTTGTGGTGGTTCA	Sigma	custom-made
Ssa4_rev GGGTTAATCGAACGGTTTGG	Sigma	custom-made
Tdh3_fwd CTCTCACTCTCCATCTTCGAT	Sigma	custom-made
Tdh3_rev CGTACCAGGAGACCAACTT	Sigma	custom-made
Tdh3_pastPolyAsite_fwd CTTGATGCGCTATTGCATTG	Sigma	custom-made
Tdh3_pastPolyAsite_rev TGTATCAGGTATCTACTACAG	Sigma	custom-made
Tlc1_pA_fwd GCCTTCGATGCATTTAGATAATTTT	Sigma	custom-made
Tlc1_pA_rev ACGCGCGATTTCTACAATAC	Sigma	custom-made
U4_fwd AGTAACCCTTCGTGGACAT	Sigma	custom-made
U4_rev AGGGGAACGCTGATCAT	Sigma	custom-made